Comparative Biochemistry and Physiology - Part D 28 (2018) 37–53

Contents lists available at ScienceDirect

Comparative Biochemistry and Physiology - Part D

journal homepage: www.elsevier.com/locate/cbpd

Transcriptomic analysis of differentially expressed genes in the molting gland (Y-organ) of the blackback land crab, *Gecarcinus lateralis*, during molt-cycle stage transitions

Sunetra Das[a,d], Lindsay Vraspir[a], Wen Zhou[b], David S. Durica[c], Donald L. Mykles[a,*]

[a] Department of Biology, Colorado State University, Fort Collins, CO 80523, United States of America
[b] Department of Statistics, Colorado State University, Fort Collins, CO 80523, United States of America
[c] Department of Biology, University of Oklahoma, Norman, OK 73019, United States of America
[d] Department of Clinical Sciences, Colorado State University, Fort Collins, CO 80523, United States of America

ARTICLE INFO

Keywords:
Crustacea
Transcriptome
Ecdysteroid
Y-organ
Molting
mTOR
Transforming growth factor - beta
Autotomy
Molt-inhibiting hormone
Neuropeptide
Cyclic nucleotide
cAMP
cGMP
Myostatin
Activin
Notch
Wnt
MAP kinase

ABSTRACT

A transcriptome of the *Gecarcinus lateralis* molting gland (Y-organ or YO) contained 48,590 contiguous sequences (contigs) from intermolt (IM), early premolt (EP), mid premolt (MP), late premolt (LP), and postmolt (PM) stages. The YO is kept in the basal state in IM by molt-inhibiting hormone (MIH)/cyclic nucleotide-dependent signaling. YO activation in EP requires down-regulation of MIH signaling and activation of mechanistic target of rapamycin (mTOR)-dependent protein synthesis. Transition of the YO to the committed state in MP requires activin/transforming growth factor-beta (TGFβ) signaling. YO repression occurs at the end of LP. A total of 28,179 contigs (58%) showed molt stage-specific changes in gene expression. The largest number of differentially-expressed genes (DEGs) were at the IM/EP (16,142 contigs), LP/PM (18,161 contigs), and PM/IM (8290 contigs) transitions. By contrast, the numbers of DEGs were 372 and 1502 contigs for the EP/MP and MP/LP transitions, respectively. DEG analysis of 23 signal transduction pathways showed significant changes in MIH, mTOR, activin/TGFβ, Notch, MAP kinase, and Wnt signaling. Down-regulation of MIH signaling genes in premolt is consistent with reduced MIH sensitivity in MP and LP. Up-regulation of mTOR signaling genes in IM and premolt stages is consistent with its role in YO activation and sustained ecdysteroidogenesis. Up-regulation of activin/TGFβ signaling genes in EP and MP is consistent with the role of a myostatin/activin-like factor in YO commitment. Notch, MAP kinase, and Wnt DEG analysis may indicate possible crosstalk with the MIH, mTOR, and activin/TGFβ pathways to integrate other inputs to control YO ecdysteroidogenesis.

1. Introduction

Molting is a complex physiological process that is essential for organismal growth of Pancrustacean species. Due to the presence of a hard exoskeleton, these animals grow discontinuously during their life cycle. In decapod crustaceans, molting is controlled by a neurosecretory center in the eyestalk ganglia, the X-organ/sinus gland (XO/SG) complex, which produces molt-inhibiting hormone (MIH) and other neuropeptides (reviewed in Hopkins, 2012; Webster, 2015). Increasing titers of ecdysteroids, synthesized by the molting gland, or Y-organ (YO), coordinate synthesis of a new exoskeleton, degradation of the old exoskeleton, limb regenerate growth, and claw muscle atrophy during the premolt stage (reviewed in Hopkins and Das, 2015; Mykles, 2001, 2011; Mykles and Medler, 2015; Skinner, 1985). The blackback land crab, *Gecarcinus lateralis*, is a well-established model for studying molting physiology, as molting can be experimentally manipulated. Molting is induced by either eyestalk ablation (ESA) or multiple leg autotomy (MLA), and molting can be suspended in early premolt by autotomy of a limb regenerate (reviewed in Chang and Mykles, 2011; Mykles, 2001; Skinner, 1985).

There are several signaling pathways that drive transitions in physiological properties of the YO over the molt cycle. MIH inhibits YO ecdysteroidogenesis during intermolt by way of a cyclic nucleotide-dependent signaling pathway involving NO synthase (NOS) and NO-dependent guanylyl cyclase (GC-I) (reviewed in Chang and Mykles, 2011; Covi et al., 2009, 2012; Webster, 2015). A reduction in MIH release from the SG initiates molting processes; the YO transitions from the basal state in intermolt (IM or stage C_4) to the activated state in

* Corresponding author.
E-mail address: Donald.Mykles@colostate.edu (D.L. Mykles).

https://doi.org/10.1016/j.cbd.2018.06.001
Received 22 April 2018; Received in revised form 23 May 2018; Accepted 7 June 2018
Available online 15 June 2018
1744-117X/

early premolt (EP or stage D_0). Increased ecdysteroidogenesis requires mTOR activity, as rapamycin, an inhibitor of mTOR Complex 1 (mTORC1; Saxton and Sabatini, 2017), suppresses YO ecdysteroid secretion in vivo and in vitro (Abuhagr et al., 2014b; Abuhagr et al., 2016). The activated YO remains sensitive to MIH and other factors (reviewed in Chang and Mykles, 2011). At mid premolt (MP or stage D_1), the animal becomes committed to molt; the transition of the YO from the activated to committed state requires a myostatin (Mstn)/activin-like transforming growth factor-beta (TGFβ)-like factor, as ESA increases *Gl-Mstn* expression in the YO and injection of SB431542, an inhibitor of activin receptor signaling, delays the increase in hemolymph ecdysteroid titers and YO expression of mTOR signaling genes in eyestalk-ablated *G. lateralis* (Abuhagr et al., 2016). During late premolt (LP or stage D_2), YO ecdysteroid synthesis reaches its highest level and hemolymph titers rise further. At the end of premolt (stage $D_{3–4}$), the YO transitions to the repressed state, in which ecdysteroidogenesis is greatly reduced and postmolt (PM) ecdysteroid titers are at their lowest (reviewed in Chang and Mykles, 2011; Mykles, 2011). It is hypothesized that YO repression results from negative feedback by the ecdysteroid peak 2–3 days before ecdysis (reviewed in Chang and Mykles, 2011).

High throughput sequencing (RNA-Seq) is a powerful tool for identifying and characterizing genes involved in physiological processes. Transcriptomes of de novo-assembled RNA-Seq data have been applied to a variety of decapod crustacean species in studies of immune and stress responses; reproduction, development, and metamorphosis; molting and limb regeneration; neurophysiology; and evolution and ecology (reviewed in Mykles et al., 2016). Comprehensive annotated transcriptomes have been generated from the YOs of *G. lateralis* and crayfish, *Pontastacus leptodactylus* (Tom et al., 2013; Das et al., 2016; Shyamal et al., 2018). Analysis of these transcriptomes identified oxidoreductases involved in ecdysteroid synthesis and metabolism (Tom et al., 2013; Shyamal et al., 2018). *G. lateralis* transcriptomes were produced from three biological replicates of YOs from intermolt animals (Das et al., 2016) and animals induced to molt by ESA (Shyamal et al., 2018). Analysis of these YO transcriptomes identified components of the MIH, mTOR, and activin/TGFβ signaling pathways, some of which were isolated previously by RT-PCR cloning (Abuhagr et al., 2014b; Das et al., 2016; MacLea et al., 2012). An unanticipated result was the large diversity of signaling pathway genes represented in both transcriptomes, including MAP kinase, Notch, Wnt, ErbB, Hedgehog, VEGF, and Jak-STAT (Das et al., 2016). These data suggest that the YO can detect and integrate a variety of physiological and environmental signals.

The goal of this study is to identify and characterize genes associated with the basal, activated, committed, and repressed states of the YO. The hypothesis is that each state represents a discrete physiological phenotype with unique gene expression profiles. A YO transcriptome was generated from the assembly of RNA-Seq data from cDNA libraries representing five molt stages: IM (stage C_4), EP (stage D_0), MP (stage D_1), LP (stage D_2), and PM (10 days postecdysis; stage B). The three IM libraries that constituted the baseline transcriptome (Das et al., 2016) were incorporated into the YO reference transcriptome reported here. The 229,278 contigs in the YO reference transcriptome were annotated and assigned to KEGG orthology pathways, including those of 23 signal transduction pathways. Relative gene expression was quantified between 5 pairwise comparisons of progressive molt stages. Global gene expression, as well as expression of 23 signal transduction pathway genes, was examined. There was a dramatic down-regulation of most genes in PM, indicating that YO was in the repressed state. There were molt stage-specific changes in MIH, mTOR, activin/TGFβ, MAP kinase, Wnt, and Notch signaling pathway genes.

2. Materials and methods

2.1. Animals and experimental treatment

Adult males of *Gecarcinus lateralis* were collected from the Dominican Republic and shipped to Colorado. Animal care and molt staging are described previously (Covi et al., 2010). Animals were induced to molt by autotomy of 8 walking legs (multiple leg autotomy or MLA) (Skinner, 1985). Hemolymph and YOs were collected from animals in one of five molt stages: IM (stage C_4), EP (stage D_0), MP (stage D_1), LP (stage D_2), and 10 days PM. Hemolymph (100 µl) was combined with 300 µl methanol and stored at −20 °C. Hemolymph ecdysteroid titers were quantified by competitive ELISA (Abuhagr et al., 2014b). Ecdysteroid titer and limb regeneration index (R-index) were used to pool the YOs for three biological replicates of each molt stage (Yu et al., 2002). YOs were stored in RNA*later* (Ambion®, California) at −20 °C.

2.2. Library preparation and sequencing

YOs from 2 to 3 individuals from the same stage were pooled for RNA isolation, cDNA synthesis, and sequencing. Total RNA was isolated using RNeasy Mini Kit (Qiagen, Maryland) (Das et al., 2016). mRNA isolation, cDNA synthesis, adapter ligation, and sequencing were conducted at the Oklahoma Medical Research Foundation Genomics facility as described (Das et al., 2016). Library preparation was based on the Illumina TruSeq stranded protocol for the Illumina HiSeq™ 2000 sequencer to generate 15 libraries containing 100 bp paired-end reads (Illumina, California).

2.3. Transcriptome assembly, annotation, and differential expression analysis

Paired-end, 100-bp reads were examined for quality using FastQC (Andrews, 2010). Reads were trimmed with Trimmomatic to remove adapters and low-quality sequences (Bolger et al., 2014). Trimmed paired and unpaired reads were assembled into contigs using Trinity (Grabherr et al., 2011). Contigs with 90% nucleotide similarity were clustered using CD-HIT-EST (Fu et al., 2012). The resulting contig database was the reference transcriptome used for downstream analysis. Trimmed reads from each library were separately aligned to the reference transcriptome using Bowtie2 for expression and to evaluate assembly quality (Langmead and Salzberg, 2012). SAMtools was used for post-processing of alignment file. Transcript expression levels (counts and FPKMs) were estimated by using eXpress tool (Roberts and Pachter, 2013). The tool versions and mapping pipeline are specified in Fig. S1.

The reference transcriptome was filtered to increase the statistical power of limma + voom in identifying differentially expressed contigs between the molt cycle stages. BLASTx searches against four databases (NCBI non-redundant, SwissProt, Uniprot-Uniref90, and Uniprot-TrEMBL) were used as input for MEtaGenome ANalyzer (MEGAN5) software to sort the hits taxonomically (Huson et al., 2007; Das and Mykles, 2016). Contigs that encoded viral or prokaryotic sequences or had count values that were disproportionately large (approximately 2 million per library) were removed. Correlations between biological replicates were first evaluated using Kendall tau's correlation coefficient. Libraries with low similarity to respective biological replicates were filtered out. From the remaining database, contigs were selected for the differential expression pipeline, with a cut-off of > 1 count per million reads in two or more libraries using edgeR v.3.16.5 (Robinson et al., 2010). The count data of the resulting filtered contigs were used for downstream analysis. The RUVSeq package (v.1.8.0) was used for normalization by identifying and removing unwanted variations using the original count data and the surrogate variable analysis (Leek and Storey, 2007; Risso et al., 2014). The limma + voom package (v.3.30.13) calculated the mean-variance of log counts for each contig

and fitted data using empirical Bayes pipelines (Law et al., 2014; Ritchie et al., 2015). The expression levels of individual genes across five molt cycle stages were analyzed using one-way ANOVA and Tukey post-hoc test on five pairwise comparisons (IM to EP, EP to MP, MP to LP, LP to PM, and PM to IM). Based on the gene-wise *p*-values, the corresponding q-values were calculated using the fdrtools R package (v.1.2.15) to identify the differentially expressed contigs. The criteria used for identifying differentially-expressed contigs were a q-value of < 0.05 and $\log_2$-fold changes of < -2 or > 2.

A comprehensive functional annotation of the YO transcriptome from intermolt *G. lateralis* was published (Das et al., 2016). Here we report for the YO the annotation of the filtered data from a differential expression pipeline over the molt cycle. KEGG (Kyoto Encyclopedia of Genes and Genomes) and KOBAS 2.0 (KEGG Orthology Based Annotation System) databases were used to identify the components of 23 signal transduction pathways. The KEGG Orthology (KO) database was downloaded from KOBAS and sequences from 7 species (*Homo sapiens*, *Drosophila melanogaster*, *Nasonia vitripennis*, *Tribolium casteneum*, *Bombyx mori*, *Ixodes sapularis,* and *Harpegnathos saltator*) were extracted. KOBAS was used to assign KO to BLASTx hits against species-specific sequences using an *E*-value cut-off < 1e-20 and Rank 1 (Xie et al., 2011). The signal transduction pathway mappings were conducted via KEGG against the reference KO database.

2.4. Computational resources and statistical analyses

The Cowboy server at Oklahoma State University was used for transcriptome assembly, expression quantification, and annotation. Filtering, differential expression, and statistical analyses were completed in RStudio Version 0.99.486 with R version 3.2.2 (64-bit). Sequence extraction and manipulation for enriched pathways used custom perl scripts (v5.22.1).

3. Results

3.1. Characterization of the de novo-assembled YO reference transcriptome from five molt stages

R-index and hemolymph ecdysteroid titer were used to determine the molt stage of MLA-induced animals. YOs were collected from individuals in IM (stage C_4), EP (stage D_0), MP (stage D_1), LP (stage D_2), or PM (stage B). There were three biological replicates for each molt stage, with each replicate consisting of RNA from two or three pairs of YOs (see Materials and Methods). Hemolymph ecdysteroid titers were low in IM (1.2 ± 0.2 pg/μl, $n = 9$), increased during premolt (EP = 21.5 ± 11.5 pg/μl, n = 9; MP = 45.4 ± 5.6 pg/μl, n = 9; LP = 130.3 ± 20.1 pg/μl, n = 9), and low in PM (1.0 ± 0.9 pg/μl, $n = 7$). The R-index ranges from zero immediately after leg autotomy to a maximum of 22–24 at the end of the premolt period (Yu et al., 2002). The R-indexes from crabs at the EP, MP, and LP stages were 14.1 ± 0.1, 16.8 ± 0.1, and 20.6 ± 0.6, respectively ($n = 9$ per stage).

Sequencing of the 15 YO libraries generated a total of 616,916,101 paired-end reads. The ~568 million reads (both paired and unpaired) that remained after trimming to remove adapters and low quality reads were de novo assembled using Trinity (Table 1; Fig. S1). The assembled transcriptome consisted of 362,494 contigs and, following elimination of redundant sequences via CD-HIT-EST, a total of 229,780 contigs constituted the YO reference transcriptome (Fig. 1). Individual reads mapped back to the reference transcriptome at an average rate of 94.2%, indicating high fidelity of the reference transcriptome assembly.

Raw counts and normalized transcript expression values as FPKM units were calculated for each contig in the reference transcriptome. Before running a differential expression package, diagnostics were conducted on the count data to remove outliers and normalize the counts across the 15 libraries. The pipeline used for differentially expressed gene (DEG) analyses is shown in Fig. 1. Using MEGAN, 1592 contigs were identified as viral or prokaryotic sequences and were eliminated from further analysis. The correlation coefficients of count data between the biological replicates indicated that the gene expression profile of the PM1 library was significantly different from the PM2 (Kendall's tau = 0.259; Pearson $R^2 = 0.117$) and PM3 (Kendall's tau = 0.259; Pearson $R^2 = 0.115$) libraries (Table S1). Consequently, the PM1 library was excluded from further analysis. Three outlier contigs with count values of > 2 million were removed from the dataset (c241624_g1_i1, c241624_g3_i1, and c196747_g1_i2). Removing other contigs with low counts resulted in a dataset with 48,590 contigs, which was designated the filtered transcriptome (Fig. 1; Table 1; see Materials and Methods). The libraries were sequenced in three separate Illumina runs, which introduced a variation that necessitated normalization of the count data. The RUVSeq package, specifically the replicate sample normalization method, was used to remove any unknown variation (Risso et al., 2014). The resulting normalized counts were used in the downstream differential expression analyses via the limma + voom package (Fig. 1). Normalization improved the statistical power based on the count data of the 14 libraries (Fig. 2 and Fig. S2). Principle component analysis (PCA) before normalization showed discrete grouping of the molt stage replicates into three distinct clusters: IM, premolt (EP, MP, and LP), and PM (Fig. 2). Normalization resulted in grouping of the EP, MP, and LP replicates into distinct subclusters (Fig. 2).

3.2. Global gene expression in the YO over the molt cycle

There were significant changes in global gene expression in the YO over the molt cycle. The five progressive pair-wise comparisons used in the DEG analysis were for the IM to EP, EP to MP, MP to LP, LP to PM, and PM to IM transitions (Fig. 3). The dataset included all 48,590 contigs in the filtered transcriptome. Parameter cut-offs for the DEG analysis were 0.05 q-value and at least a 4-fold change, in order to focus on those contigs that showed significant changes in the pair-wise comparisons. Volcano plots showed changes in relative expression for the IM/EP, EP/MP, MP/LP, LP/PM, and PM/IM transitions (Fig. 3A). A total of 28,179 unique contigs, or 58%, of the filtered transcriptome was identified as differentially expressed between at least one pair-wise comparison, but the number and percentage varied between the five pairwise comparisons. The total number of DE contigs ranged from a low of 372 (1%) contigs for the EP/MP transition to 18,161 (65%) contigs for the LP/PM transition (Fig. 3B). The number of DE contigs was 16,142 (57%) for the IM/EP transition; 1502 (5%) for the MP/LP transition; and 8281 (29%) for the PM/IM transition (Fig. 3B). There were significant differences in the number of up- and down-regulated DE contigs between the molt stage comparisons (Fig. 3B). For the IM/EP comparison, 11,324, or 70%, of the 16,142 contigs were down-regulated (Fig. 3B). By contrast, a majority of the DE contigs was up-regulated in the next three molt stage comparisons: 283 (76%) for EP/MP; 1272 (85%) for MP/LP; and 12,595 (69%) for LP/PM (Fig. 3B). For the PM/IM comparison, 3852 (47%) of the 8281 DE contigs were up-regulated (Fig. 3B). Of the 28,179 unique DE contigs, only 19 had significant changes in expression levels in all five transitions (data not shown).

Of the 28,179 DE contigs, 13,379 contigs, or 48%, were annotated by Trinotate and BLAST (see Materials and Methods; Fig. 1). The number and percentage of the annotated DE contigs differed significantly between the molt stage comparisons: 7668 (48%) for IM/EP; 189 (51%) for EP/MP; 225 (15%) for MP/LP; 8275 (46%) for LP/PM; and 4502 (54%) for PM/IM (Fig. 3B). Moreover, there were also significant differences in the proportion of up- and down-regulated annotated and non-annotated DE contigs. The percentages of up-regulated non-annotated contigs ranged between 17% for PM/IM and 76% for MP/LP (Fig. 3B). The percentages of down-regulated non-annotated contigs ranged between 9% for EP/MP and MP/LP to 34% for IM/EP (Fig. 3B).

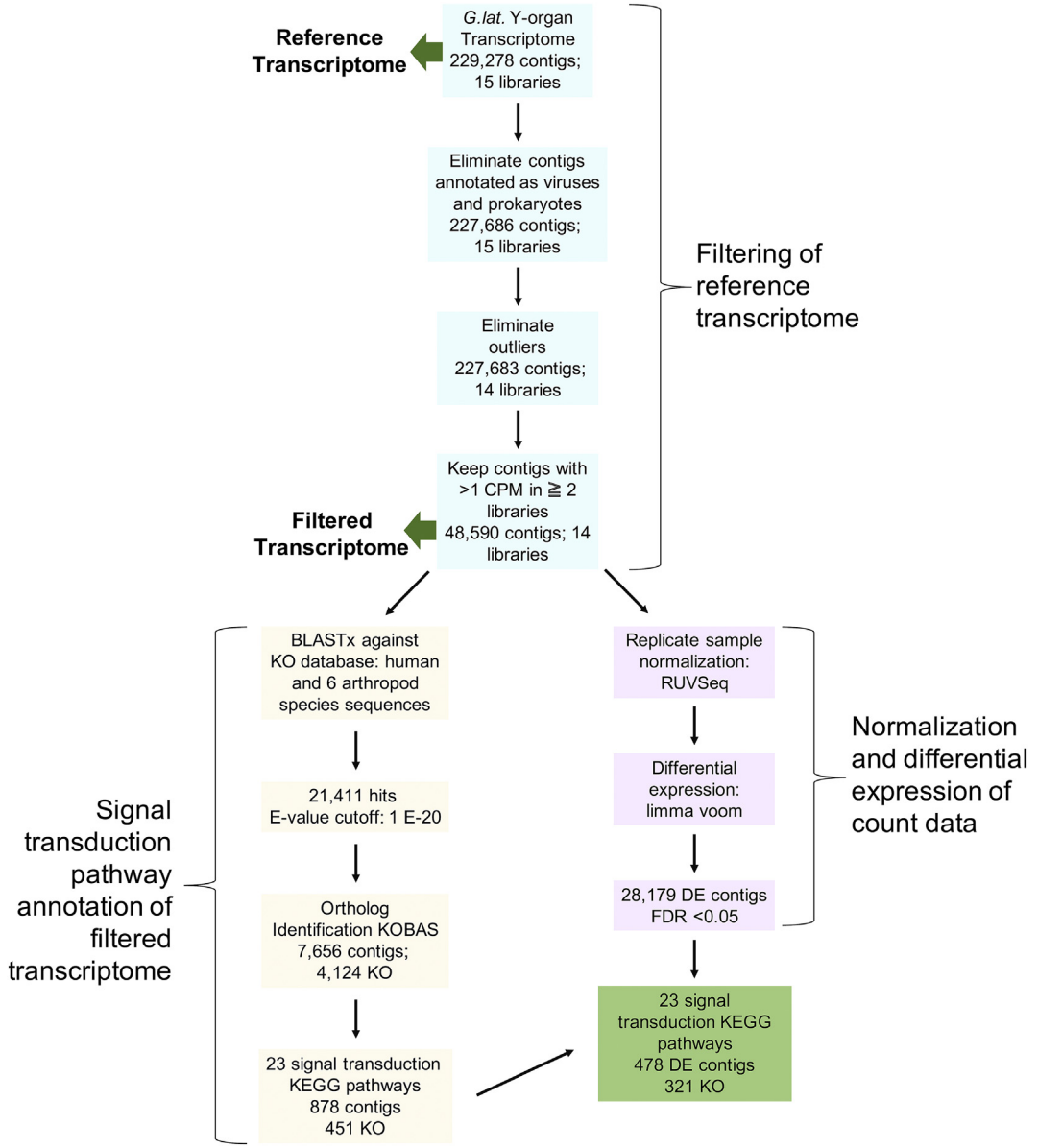

Fig. 1. Differential expression pipeline. There are three distinct bioinformatic processes (represented in three different colors) used to identify the differentially expressed (DE) signal transduction genes. Following filtering of outliers and low counts, the data was processed simultaneously for signal transduction gene annotation and identification of DE contigs. The processes and results are included in each box.

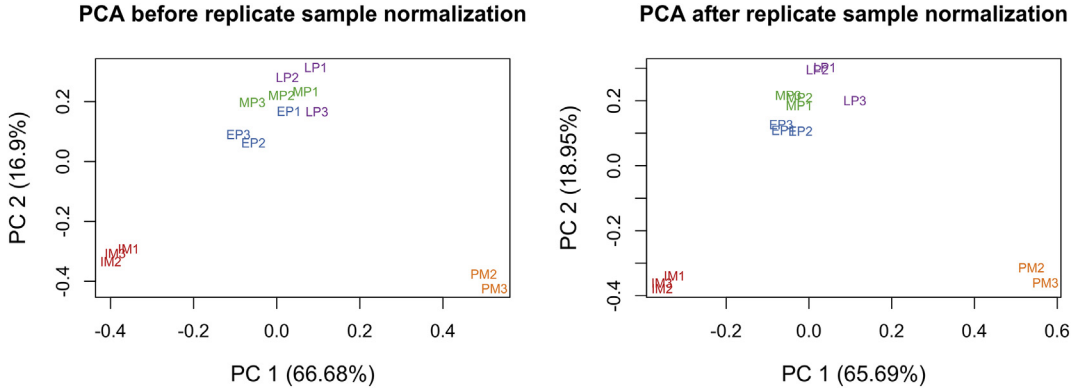

Fig. 2. Principle component analysis (PCA) of Y-organ libraries from five molt cycle stages. Following normalization of count data, the corresponding PCA shows segregation of molt cycle stages based on the expression profile of each library. Abbreviations: IM, intermolt; EP, early premolt; MP; mid premolt; LP, late premolt; and PM, postmolt.

Table 1
Statistics on Illumina sequencing output and analyses of the YO transcriptome.

Sequencing and mapping statistics	
Total number of raw reads	616,916,101
Total number of trimmed reads	568,373,909
Total number of contigs following trinity assembly	362,494
Total number of contigs following clustering (reference transcriptome)	229,278
Contigs with CPM of > 1 in ≥2 libraries (Filtered transcriptome)	48,590
Reference transcriptome statistics	
Median contig length (N50)	1082 bp
Average contig length	680 bp
Number of annotated contigs	67,355 (29.4%)
Filtered transcriptome statistics	
Median contig length (N50)	1537.79 bp
Average contig length	2347 bp
Number of annotated contigs	23,030 (47.4%)

The data in Fig. 3 are presented as relative expression; it does not represent absolute changes in contig levels. Displaying only relative expression of the DEG data will not reveal biologically significant changes in absolute levels. Table S2 compares the median and mean transcript abundance (FPKM) as indicators for the distribution of the DE contig levels in the datasets of the five molt stage comparisons. The means were greater than the medians in all stages, which indicated that the data were skewed by a relatively small number of contigs that were expressed at high levels. In other words, most of the DE contigs were expressed at lower levels. The medians differed between the molt stages, ranging between 0 FPKM for the PM stage in the LP/PM and PM/IM comparisons and 14.3 FPKM for the LP stage in the MP/LP comparison (Table S2). The PM stage had the largest numbers and percentages of DE contigs with an FPKM of zero: 14,067 (77%) for the LP/PM comparison and 5607 (68%) for the PM/IM comparison (Table S2). Moreover, 97% and 99% of the PM contigs in the LP/PM and PM/IM comparisons, respectively, had FPKMs of < 5 (Table S2). By contrast, the numbers of the DE contigs with 0 FPKM ranged from 6 to 532 for the molt stages in the IM/EP, EP/MP, and MP/LP comparisons (Table S2). The LP stage for the LP/PM comparison had 1875 DE contigs (10%) with 0 FPKM and 13,687 DE contigs (75%) with < 5 FPKM (Table S2).

3.3. Differential expression of signaling pathway genes

A goal was to identify signaling pathway genes that are associated with molt stage transitions of the YO. KEGG orthologs (KO) analysis was used to annotate all contigs from the filtered transcriptome dataset (48,590 contigs) to map the contigs to signal transduction pathways. Following BLASTx against sequences from seven species, 7656 contigs were assigned KO terms (Fig. 1). Of these annotated contigs, 878 (11%) were mapped to 23 KEGG signal transduction pathways (Table 2). There was a total of 478 (54%) contigs that were differentially expressed (Table 2). Almost all (96%) of the 279 DE contigs in the transition from IM to EP were down-regulated (Table 3). There were relatively few DE contigs in the EP/MP and the MP/LP comparisons. Five of the five DE contigs for EP/MP and one of the four DE contigs for MP to LP were down-regulated (Table 3). For the LP/PM and PM/IM comparisons, 88 (31%) and 41 (22%) contigs were down-regulated, respectively. A heatmap was generated to show the relative expression profiles of the 478 DE contigs over the molt cycle (Fig. 4). There were three general profiles. Many of the contigs showed highest relative expression in IM, decreasing expression during premolt, and lowest relative expression in PM (profile 1). Some contigs showed sustained expression at IM, EP, MP, and LP and low expression at PM (profile 2), while others showed highest relative expression in EP (profile 3) (Fig. 4).

MIH maintains the YO in the basal state during the IM stage. A reduction in MIH release from the SG initiates YO activation and the animal transitions from IM to EP. The proposed MIH signaling pathway includes adenylyl cyclase (*adcy*), protein kinase A (*pka*), nitric oxide synthase (*nos*), guanylyl cyclase I (*gcI*), calmodulin (*calm*), calcineurin (*caln*), and protein kinase G (*pkg*) (reviewed in Chang and Mykles, 2011). All the components of proposed MIH signaling pathway, as well as *elongation factor 2* (*ef2*) and *guanylyl cyclase-III* (*gcIII*), were recovered from the transcriptome. Three full-length contigs encoding *adcy* (*adcy1*, *adcy2*, and *adcy9*) were recovered. The sequences of the *ef2*, *nos*, *gcI*, and *gcIII* contigs were the same as the *Gl-EF2*, *Gl-NOS*, and *Gl-GC-III* sequences obtained by RT-PCR (Kim et al., 2004; Lee et al., 2007b). GC-I is an NO-dependent GC and GC-III is a constitutively active GC that may support GC-I function (Lee et al., 2007a). Seven (*adcy1*, *adcy2*, *adcy9*, *nos*, *pka*, *caln*, and *pkg*) of the 10 contigs were expressed at their highest levels in IM (Figs. 5A, 6A). *Calm* level increased during premolt and decreased at PM. There was no effect of molt stage on *gcI* and *gcIII* levels (Figs. 5A, 6A). All ten contigs were expressed at their lowest levels in PM.

YO activation and sustained ecdysteroid synthesis requires mTOR activity. The 17 mTOR signaling components recovered from the YO transcriptome were *akt* (protein kinase B), autophagy related 1 (*atg1*), cap-gly domain containing linker 1 (*clip1*), frizzled 1/7 (*fzd1_7*), growth factor receptor bound protein 2 (*grb2*), insulin-like growth factor 1 receptor (*igf1r*), late endosomal/lysosomal adaptor, MAPK and mTOR activator 3 (*lamtor3*), mechanistic target of rapamycin (*mtor*), phosphatase and tensin homolog (*pten*), regulatory associated protein of mTOR complex 1 (*raptor*), rapamycin-insensitive companion of mTOR (*rictor*), ras homolog enriched in brain (*rheb*), S6 protein kinase (*s6 k*), STE20-related kinase adaptor alpha (*strada*), tuberous sclerosis complex 2 (*tsc2_a* and *tsc2_b*), and eukaryotic translation initiation factor 4E binding protein 1 (*ef4ebp*). The sequences of *akt*, *mtor*, *rheb*, and *s6 k* were the same as the *Gl-Akt*, *Gl-mTOR*, *Gl-Rheb*, and *Gl-S6K* sequences obtained by RT-PCR (MacLea et al., 2012; Abuhagr et al., 2014b). The KEGG pathway with the DE components is shown in Fig. 8A. Six contigs (*atg1*, *ige1r*, *tsc2_a*, *grb2*, *ef4ebp*, and *lamtor3*) were expressed at their highest levels in IM (Figs. 5B, 6B). Seven contigs (*mTOR, raptor*, *rictor*, *s6 k*, *strada*, *akt*, and *clip1*) were expressed at high levels in both IM and EP (Figs. 5B, 6B). *Rheb* and *tsc2_b* contig levels were significantly increased from IM to EP and remained elevated in MP and LP (Figs. 5B, 6B). Only two contigs (*fzd1_7* and *pten*) were not differentially expressed over the molt cycle (Figs. 5B, 6B). All 17 contigs were expressed at their lowest levels in PM.

Activin/TGFβ signaling drives the transition of the YO from the activated to committed state at MP. The activin/TGFβ contig sequences retrieved from the YO transcriptome were myostatin-like (*mstn*), activin receptor 1 (*acvr1*), R-Smad (*smad2_3*), Co-Smad (*smad 4*), I-Smad (*smad6*), and bone morphogenetic protein (BMP) and activin membrane-bound inhibitor (*bambi*) (Fig. 8B). The sequence of *mstn* was the same as the *Gl-Mstn* sequence obtained by RT-PCR (Covi et al., 2008). *Acvr1*, *smad6*, and *mstn* contigs were expressed at higher levels in IM and EP, although the means were not always statistically significant (Figs. 5C, 6C). *Smad2_3* and *smad4* contig levels were highest in EP and MP (Figs. 5C, 6C). *bambi* was expressed highly in IM and was significantly down-regulated in premolt stages (Figs. 5C, 6C). Contigs encoding genes from other TGFβ signaling pathways were also retrieved: BMP7 (*bmp7*), BMP receptor 1B (*bmpr1b*), chordin (*chrd*), CREB binding protein (*crebbp*), cullin 1 (*cul1*), and R-Smad (*smad1*) (Fig. 8B). Five contigs (*bmpr1b*, *chrd*, *crebbp*, *bmp7*, and *cul1*) were expressed at their highest levels in IM and were significantly down regulated in the premolt stages (Figs. 5C, 6C). *Smad1* was expressed at higher levels in IM and EP (Figs. 5C, 6C). The levels of all 12 contigs were lowest in PM.

The PM YO is in the repressed state. Although most the DE genes were expressed at low levels in PM, the hierarchical clustering of the signal transduction DE contigs (Fig. 4) identified four genes that were expressed only in PM: *diacylglycerol kinase alpha* (*dgkA*), *enolase* (*eno*),

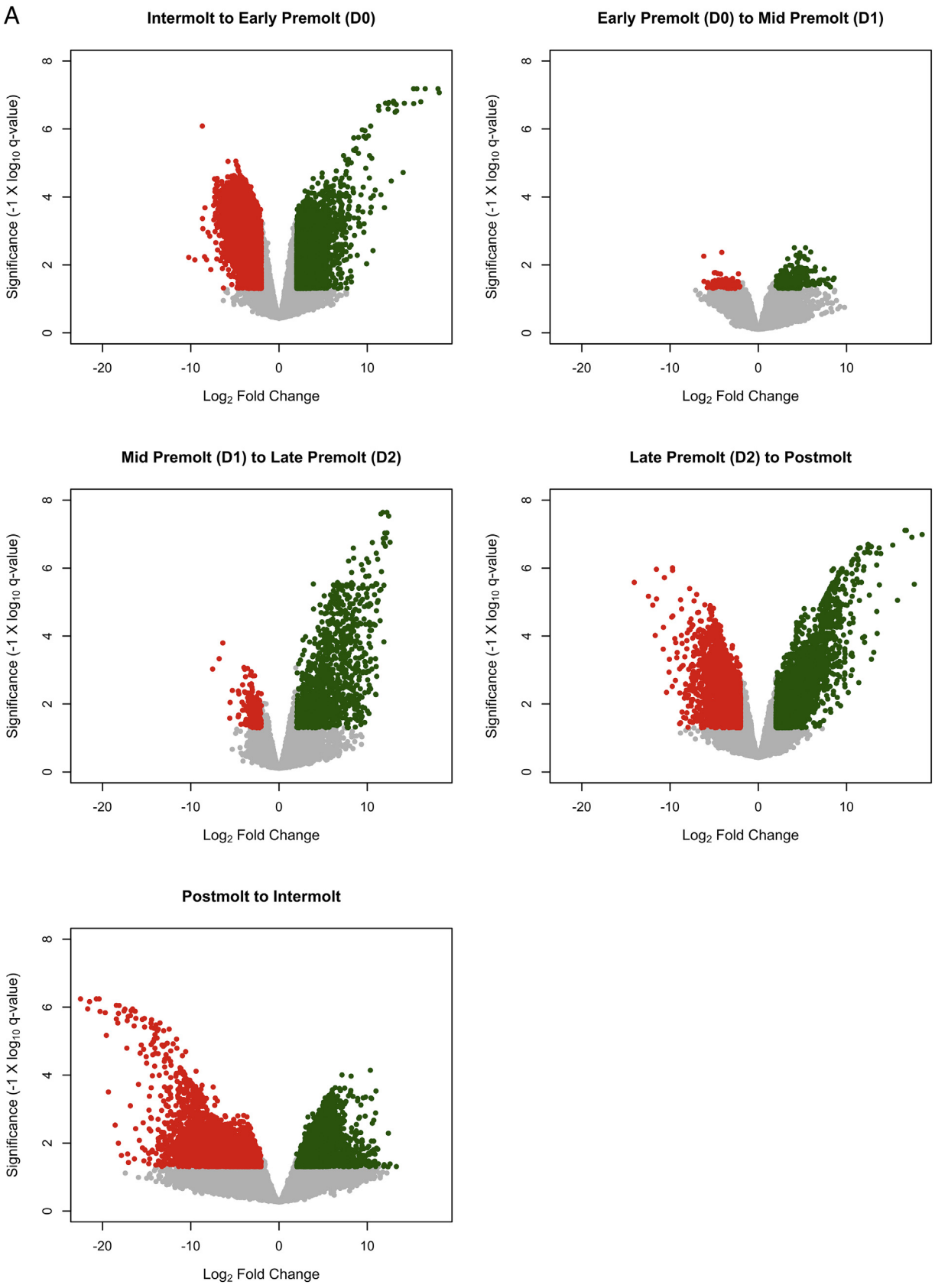

Fig. 3. Effects of molt stage on the levels of differentially-expressed contigs in the filtered YO transcriptome. (A) Volcano plots of the DE contigs q-value as a function of $\log_2$ fold change. The cut-off used for identifying the DE contigs were: q-value < 0.05 and $\log_2$ fold change < -2 or $> +2$. The five pairwise comparisons used in this analysis are: IM to EP; EP to MP; MP to LP; LP to PM; and PM to IM. The DE contigs that have a negative fold change are indicated in red and DE contigs with a positive fold change are indicated in green. (B) Graphical representation of the number of DE contigs in each comparison. The number and percentage of annotated and not-annotated contigs are represented in green for up-regulated contigs and in red for down-regulated contigs. (For interpretation of the references to colour in this figure legend, the reader is referred to the web version of this article.)

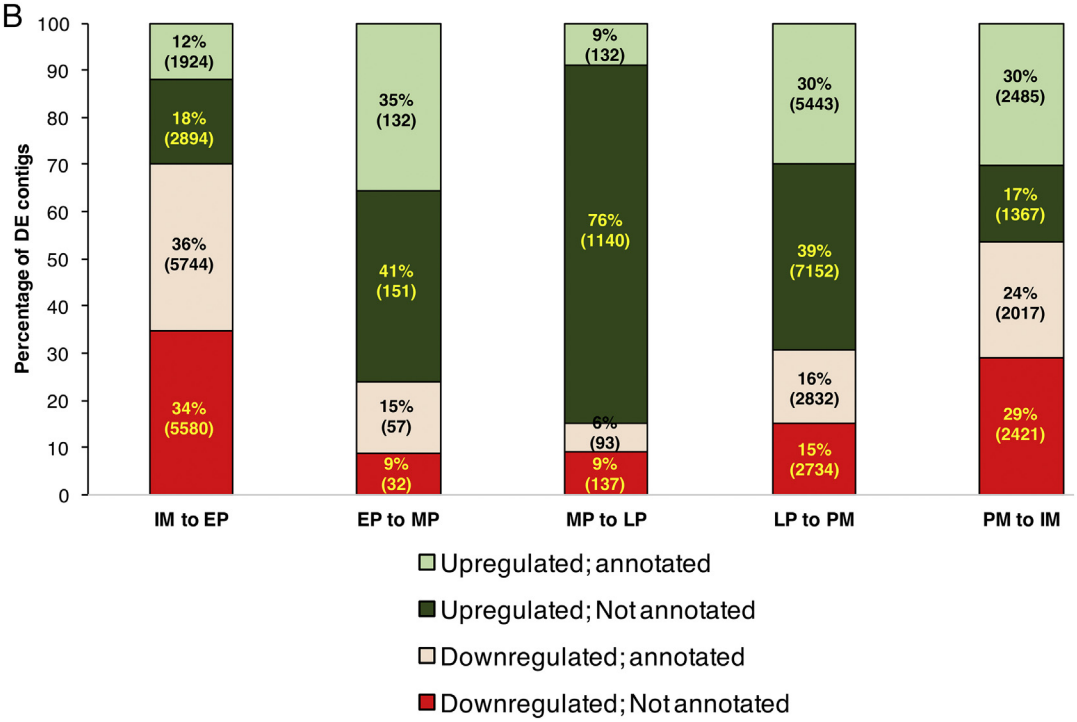

Fig. 3. (*continued*)

Table 2
Number of total and differentially expressed annotated contigs assigned to KEGG signal transduction pathways.

Signaling pathway	Pathway ID	Number of annotated contigs	Number of DE contigs (percentage)
AMPK signaling pathway	k04152	86	53 (62%)
Calcium signaling pathway	k04020	92	49 (53%)
cAMP signaling pathway	k04024	104	65 (63%)
cGMP-PKG signaling pathway	k04022	94	51 (54%)
ErbB signaling pathway	k04012	48	24 (50%)
FoxO signaling pathway	k04068	79	46 (58%)
Hedgehog signaling pathway	k04340	36	21 (58%)
HIF-1 signaling pathway	k04066	50	26 (52%)
Hippo signaling pathway	k04390	95	52 (55%)
Jak-STAT signaling pathway	k04630	26	12 (46%)
MAPK signaling pathway	k04010	106	66 (62%)
mTOR signaling pathway	k04150	92	54 (59%)
NF-kappa B signaling pathway	k04064	33	16 (48%)
Notch signaling pathway	k04330	28	17 (61%)
Phosphatidylinositol signaling system	k04070	86	47 (55%)
Phospholipase D signaling pathway	k04072	83	50 (60%)
PI3K-Akt signaling pathway	k04151	128	69 (54%)
Rap1 signaling pathway	k04015	115	63 (55%)
Ras signaling pathway	k04014	105	57 (54%)
Sphingolipid signaling pathway	k04071	98	60 (61%)
TGF-beta signaling pathway	k04350	32	18 (56%)
TNF signaling pathway	k04668	40	23 (58%)
Wnt signaling pathway	k04310	79	51 (65%)

troponin-C_2 (*tnnc2*), and *htG* (*hsp90*) (Table S4). These genes, which are components of the phospholipase D, HIF-1, calcium, and PI3K-Akt signaling pathways, respectively, had comparatively low or no expression in the IM and premolt stages. The expression levels of these genes ranged between 0.04 and 3.16 FPKM in PM (see supporting data). All four genes were differentially expressed in the LP/PM and PM/IM transitions.

Table 3
Differentially expressed signal transduction pathway contigs between pair-wise molt stage comparisons.

Stage comparison	Number of contigs up-regulated	Number of contigs down-regulated
IM/EP	11 (4%)	268 (96%)
EP/MP	0 (0%)	5 (100%)
MP/LP	3 (75%)	1 (25%)
LP/PM	195 (69%)	88 (31%)
PM/IM	143 (78%)	41 (22%)

Heatmaps revealed three profiles of the changes in relative expression levels of the 39 genes in the MIH, mTOR, and TGFβ signaling pathways (Fig. 6). Profile 1 was exhibited by 19 contigs; levels were highest in IM, decreased in EP, and remained low in MP, LP, and PM. These included *adcy1*, *adcy2*, *adcy9*, *caln*, *nos*, *pka*, and *pkg* in the MIH pathway (Fig. 6A); *atg1*, *grb2*, *igf1r*, *lamtor3*, *s6 k*, and *tsc2_a* in the mTOR pathway (Fig. 6B); and *bambi*, *bmp7*, *bmpr1b*, *chrd*, *crebbp*, and *cul1* in the TGFβ pathway (Fig. 6C). Profile 2 showed sustained expression in IM and premolt stages and low expression in PM. These included *gcI* in the MIH pathway (Fig. 6A); *akt*, *clip1*, *mtor*, *rictor*, *pten*, *ef4ebp*, and *s6 k* in the mTOR pathway (Fig. 6B); and *smad1* and *smad6* in the TGFβ pathway (Fig. 6C). Profile 3 showed higher expression in premolt stages. Contigs in this profile were *gcIII* and *calm* in the MIH pathway (Fig. 6A); *fzd1_7*, *raptor*, *rheb*, *strada*, and *tsc2_b* in the mTOR pathway (Fig. 6B); and *acvr1*, *mstn*, *smad2_3*, and *smad4* in the TGFβ pathway (Fig. 6C).

Using the changes in specific genes, heatmap, and percentage of DE contigs as criteria, we identified several other pathways that were associated with molt cycle stage transitions. Of the 23 pathways analyzed, the MAPK (62%), Notch (61%), and Wnt (65%) signaling pathways had the largest percentages of their respective components that were differentially expressed (Table 2). The three expression profiles for most of

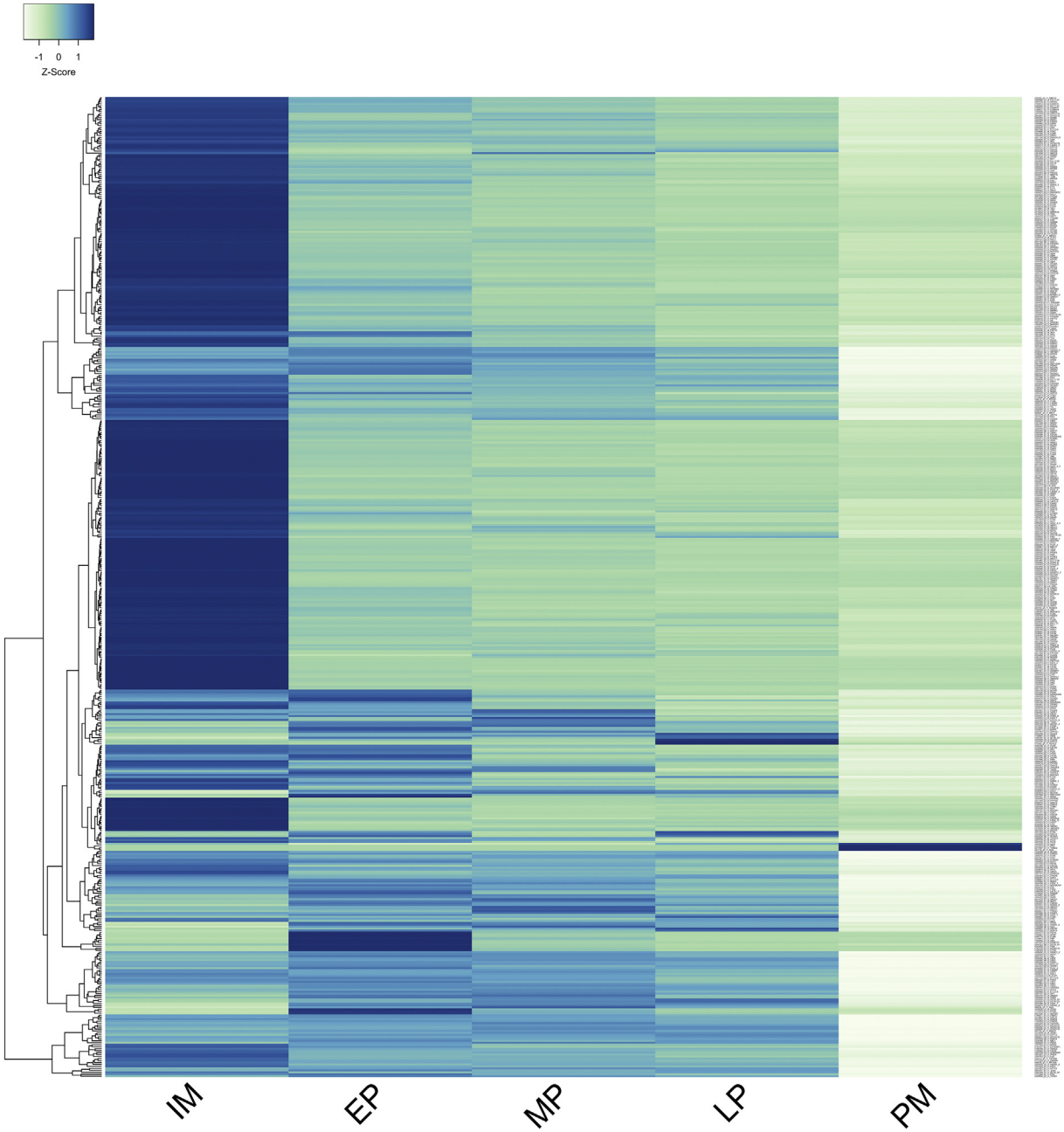

Fig. 4. Heatmap of 478 DE contigs that were annotated as components of signal transduction pathways. The average log FPKM values were used to show the expression profile of DE contigs across five molt cycle stages. The expression of the majority of the contigs was highest in IM and lowest in PM. Relatively fewer DE contigs were identified in the transitions from EP to MP and MP to LP.

the MAPK, Wnt, and Notch genes were the same as those observed for the MIH, mTOR, and TGFβ signaling genes: highest expression in IM, lower in premolt, and lowest in PM (profile 1); sustained expression in IM and premolt and low in PM (profile 2); and highest expression in EP (profile 3) (Fig. 7). Twelve of the 19 MAPK signaling contigs (*rras2_b, nfkb2, grb2, rapgef2, mek1, nf1_a, nf1_b, ikbka, ikbkb*, *mnk,* and, *sos*) showed expression profile 1, four contigs (*egfr, nf1_c, fgfr2*, and, *rap1A*) showed profile 2, and three contigs (*mras, s6kA-P3,* and, *kras*) showed profile 3 (Fig. 7A). Fifteen of the 28 Notch signaling contigs (*adam17, aph1, fng, cir, numbl, groucho, pen2, crebbp, aph1, ctbp, snw1, jagged, adam17, notch,* and, *adam17)* showed expression profile 1; 8 contigs (*numbl_a, rbpsuh, dvl, pcaf, numbl_c, dtx, notch_a,* and, *psen1*) showed profile 2; and 3 contigs (*ncstn_a, hdac1,* and *ncstn_b)* showed profile 3 (Fig. 7B). The *jagged* and *nstcn* had highest expression in MP (Fig. 7B). Ten of the 29 Wnt signaling contigs (*csnk1a, csnk1e_a, csnk1e_b, nlk_a, nlk_b, lrp5_6, groucho_a, fzd9_10, ppn,* and, *rvbl*) showed expression profile 1, 11 contigs (*gsk2B, dvl, axin1, fzd_7_a, csnk2A_a, csnk2A_b, csnk2B, ctnnB1, groucho_b, tak1,* and, *txf7L2_b*) showed profile 2, and six contigs (*fzd1_7_b, fzd1_7_c, fzd4, fzd5, wnt4,* and, *tcf7L2_a*) showed profile 3 (Fig. 7C). In addition, *wnt*5 and *wnt7* had highest expression levels in LP stage (Fig. 7C).

The dataset was used to identify markers for specific molt stages. As mentioned in the global gene expression analyses, only 30% of the contigs were up-regulated in the transition from IM to EP. Using the data from KEGG analyses of signal transduction pathways, 11 contigs were identified that were significantly up-regulated in EP (Tables 3, S3). These genes were components of the mTOR, AMPK, PI3K-Akt, calcium, Notch, MAPK, Hippo, and Wnt signaling pathways. There were five genes (*V-type H^+-transporting ATPase subunit G, amyloid beta A4 precursor protein-binding family B member 1-interacting protein, speckle-*

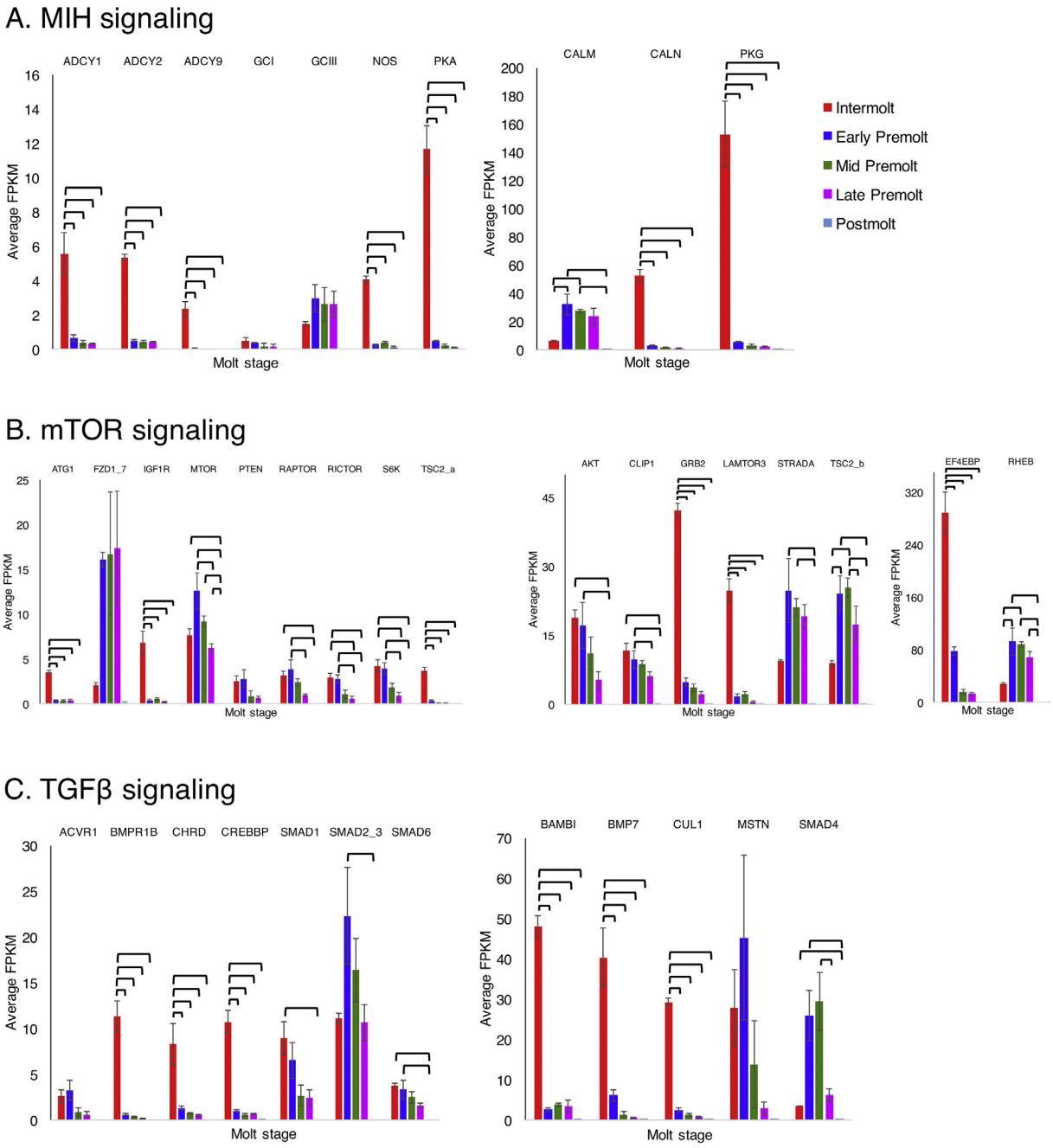

Fig. 5. Expression levels of selected components from the MIH (A), mTOR (B), and TGFβ (C) signaling pathways. DE genes were identified via ANOVA and post-hoc Tukey test ($P < 0.05$). A total of 40 genes were selected from these three pathways, 34 of which were differentially expressed. Brackets indicate significant differences between means ($P < 0.05$).

type POZ protein, *phosphatidylinositol 4-kinase A*, and *eukaryotic translation initiation factor 4E binding protein 1*) that were significantly down-regulated from EP to MP. The transition from MP to LP led to significant changes in expression of four genes (*tyrosine-protein kinase Src, guanine nucleotide-binding protein subunit alpha-14, secretory phospholipase A2,* and *serine/threonine-protein phosphatase PP1 catalytic subunit*) (Table 3). There were 195 genes that were significantly up-regulated from LP to PM (Table 3), but only four genes had FPKM values > 1 (Table S4). Thus, there were a total of 24 genes that were up- or down-regulated at specific molt stages and may collectively be used as markers for distinguishing the YO states over the molt cycle.

4. Discussion

A transcriptomics approach was used to analyze gene expression in the YO at five discrete stages of the molt cycle. Gene expression profiles and percentage of DE contigs in the KEGG pathway analyses were used as criteria for identifying signaling genes associated with YO activation, commitment, and repression. Global changes in gene expression that included annotated and non-annotated contigs revealed two important findings: (1) YO activation was associated with the down-regulation of a large number of genes (11,324 genes for IM/EP), while YO commitment was associated with the up-regulation of a small number of different genes (283 genes for EP/MP) and (2) expression of most genes was lowest in the PM stage when compared to other stages (Figs. 3, 4). A lower number of DE contigs were identified in the EP/MP transition

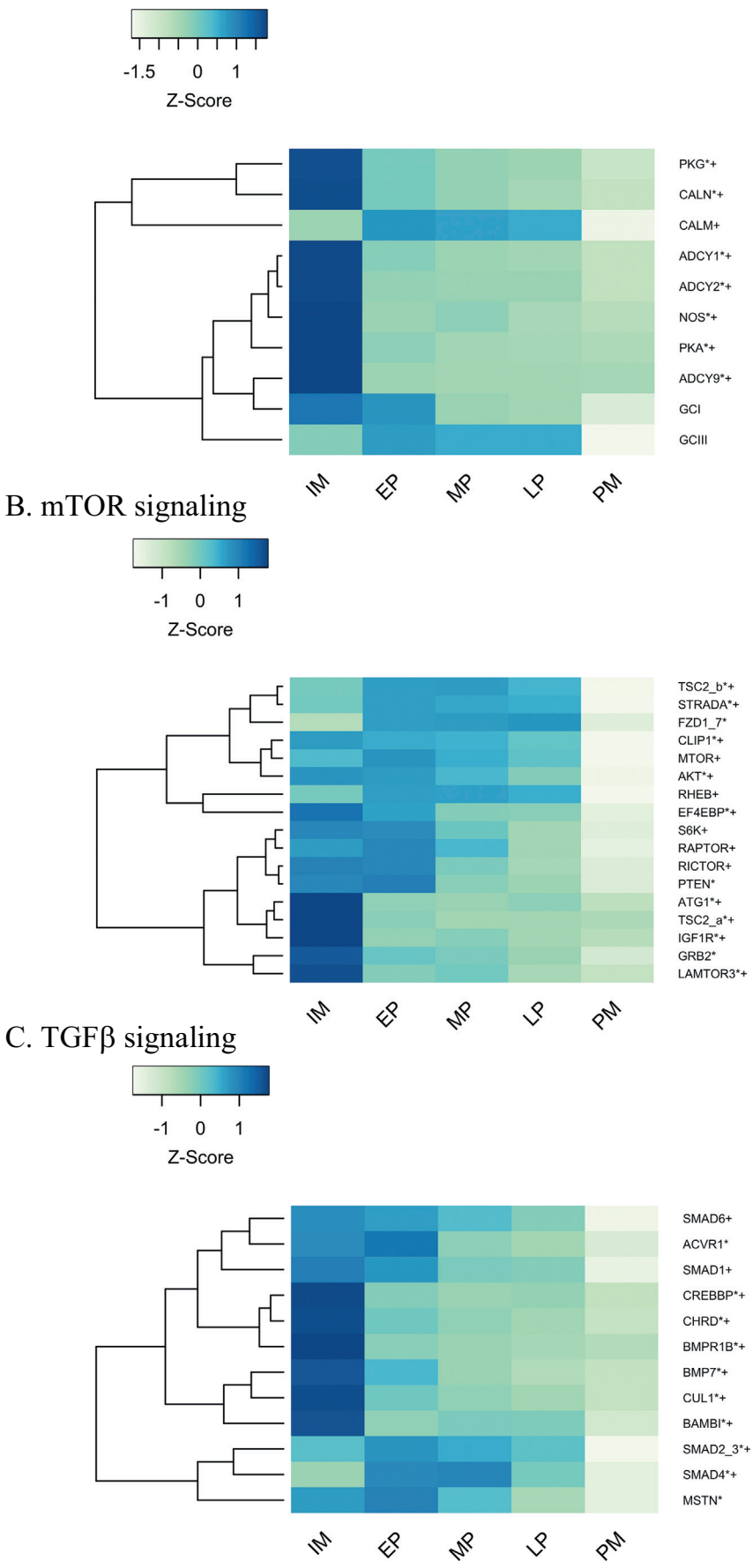

(caption on next page)

Fig. 6. Heatmap of the expression of genes in the MIH (A), mTOR (B), and TGFβ (C) signaling pathways. DE contigs identified by limma-voom analyses are marked with an asterisk by the gene name. DE contigs identified by ANOVA are marked with a plus sign.

when compared to the IM/EP, MP/LP, LP/PM, and PM/IM transitions (Fig. 3B). The PCA analysis showed three major groupings consisting of IM, PM, and premolt (EP, MP, and LP) libraries (Fig. 2). The proximity of the nine premolt libraries in the PCA analysis indicated that the gene expression profiles of the EP, MP, and LP stages were more similar to each other than they were to either the IM or PM libraries, although the EP, MP, and LP libraries formed distinct groupings after normalization (Fig. 2). This suggests that, in terms of global gene expression, there were three major transitions: IM to EP; LP to PM; and PM to IM. In other words, YO activation (IM/EP), repression (LP/PM), and restoration of the basal state (PM/IM) were associated with the largest changes in gene expression. YO commitment (EP/MP transition) was associated with a relatively small number of DE contigs. As many of these genes were non-annotated (52% of the DE genes in IM/EP; 50% in EP/MP; 85% in MP/LP; 54% in LP/PM, and 46% in PM/IM), their roles in YO control cannot be assessed.

Most of the contigs from the IM and premolt YOs were expressed at very low levels in PM. The average contig level, expressed as FPKM, for the PM stage was skewed towards zero. Even though contigs with low counts were removed before DE analysis of the filtered transcriptome (Fig. 1), 78% and 83% of the 48,590 contigs in the PM2 and PM3 datasets, respectively, had a count value of zero. The statistical tools used for the DE analysis usually demand removal of contig samples with zero count values. However, this would have eliminated 80% of the contigs that had higher count values in the other four molt stages from the analysis. Although the LP/PM transition had the highest number of DE contigs (18,161; Fig. 3B), the median FPKM was 0 in PM and 0.5 in LP (Table S2). In comparison, the next highest number of DE contigs (16,142) was identified in the IM/EP transition. The median FPKM of the 16,142 DE contigs was 3.5 in IM and 0.8 in EP (Table S2). Although 30% of the DE contigs in the IM/EP transition were up-regulated, only 3% of the 16,142 DE contigs were at 0 FPKM in EP stage (Table S2). By contrast, 77% of the DE contigs were at 0 FPKM in the PM stage, even though 69% of the DE contigs were up-regulated in the LP/PM transition (Table S2). Expression of the DE data as relative fold change in levels can be misleading, as it does not take into account the absolute count values (Fig. 3). Two contigs can show the same-fold change in expression, but can have different FPKM values. As a hypothetical example, contig #1 may increase from 0.01 to 0.1 FPKM and contig #2 may increase from 1 to 10 FPKM. Both have a 10-fold increase in expression, but the difference in FPKM would be 0.09 for contig #1 and 9 for contig #2. FPKM values that are at or near zero would distort the DE analysis, so that statistically significant changes may not be biologically meaningful. Most of the contigs that were up-regulated in PM had low FPKM values in the LP stage. By contrast, most of the down-regulated genes in the PM stage were expressed at high levels in the IM and premolt stages; these include the MIH, mTOR, and TGFβ signaling genes (Fig. 5). These data suggest that transcriptional rates are lower in the repressed YO, which corresponds to its low ecdysteroidogenic activity in postmolt (see below).

Intermolt is the molt stage that an animal is not actively engaged in the preparation for, or recovery from, ecdysis. It can vary in duration from months to years in adult decapod crustaceans, depending on nutritional and environmental conditions (reviewed in Aiken and Waddy, 1992; Green et al., 2014; Skinner, 1985). Low hemolymph ecdysteroid titers are maintained in IM animals by sustained inhibition of the YO by the pulsatile release of MIH from the XO/SG complex in the eyestalk ganglia (reviewed in Chang and Mykles, 2011; Skinner, 1985; Webster et al., 2012). The basal YO is characterized by low ecdysteroid synthesis and high sensitivity to MIH (reviewed in Nakatsuji et al., 2009; Webster et al., 2012). Binding of MIH to a membrane receptor initiates a signaling cascade mediated by cyclic nucleotide second messengers (reviewed in Covi et al., 2009). The current model links a cAMP/Ca^{2+}-dependent phase triggered by MIH binding and a NO/cGMP-dependent summation phase, which inhibits ecdysteroidogenesis between MIH pulses (reviewed in Chang and Mykles, 2011; Covi et al., 2012; Webster, 2015). A Ca^{2+}/CaM-dependent NO synthase has a key role in transmitting and amplifying the triggering signal (Kim et al., 2004; Mykles et al., 2010). NOS is activated by the combined actions of direct binding of Ca^{2+}/CaM and dephosphorylation by calcineurin, a Ca^{2+}/CaM-dependent protein phosphatase (Lee and Mykles, 2006); reviewed in Chang and Mykles, 2011; Covi et al., 2012). All the components of the MIH signaling pathway are expressed in the YO (Kim et al., 2004; Lee et al., 2007a; Lee et al., 2007b; Abuhagr et al., 2014a; Das et al., 2016; Pitts et al., 2017) (Table 2, Fig. 5A). In insects, NO mediates the inhibition of the PG by regenerating tissues (reviewed in Andersen et al., 2013; Hackney and Cherbas, 2014). In *Manduca sexta*, NO donor DETA-NONOate inhibits PG ecdysteroid secretion (DeLalio et al., 2015). Dilp8, an ILP secreted by damaged imaginal discs, activates NOS in *Drosophila* PG by binding to relaxin receptor homolog (Lgr3), a G protein-coupled receptor, to inhibit ecdysteroid synthesis (Jaszczak et al., 2015; Jaszczak et al., 2016). Thus, NOS activity inhibits ecdysteroidogenesis in the molting glands of both insects and crustaceans, but is controlled by different factors.

The expression of MIH signaling genes is correlated with changes in YO sensitivity to MIH over the molt cycle. The YO becomes less sensitive to MIH in early premolt and is refractory to MIH in mid to late premolt when the animal is committed to molt (Chung and Webster, 2003; Nakatsuji and Sonobe, 2004; Nakatsuji et al., 2006); reviewed in Nakatsuji et al., 2009). There was a large decrease in the expression of seven of the 10 genes in the MIH signaling pathway from IM to EP; expression of *acdy1/2/9*, *pka*, *caln*, *nos*, and *pkg* remained low in premolt stages and then dropped to lowest levels in PM (Figs. 5A, 6A). By contrast, the expression of *calm* was higher in premolt (Figs. 5A, 6A). There was no effect of molt stage on the expression of NO-dependent GC (*gc-I*) and NO-independent GC (*gc-III*) (Figs. 5A, 6A). These data indicate that there is a lag between MIH signaling gene expression and YO sensitivity to MIH; reduced mRNA levels in the activated YO in EP precede the reduced MIH sensitivity of the committed YO in MP and LP. Presumably, a low turnover of MIH signaling proteins contributes to this lag. Conversely, high expression of MIH signaling genes correlates with high YO sensitivity to MIH in IM animals, and even higher expression levels may confer hypersensitivity under certain conditions. Some *G. lateralis* individuals are refractory to molt induction by MLA and are considered “blocked”; individuals show no signs of molting three months after MLA (Pitts et al., 2017). The mRNA levels of five of the 10 MIH signaling genes quantified in the YO from these individuals are two to four orders of magnitude higher than those in the YO of control individuals, suggesting that the YO can be inhibited by low MIH levels in the hemolymph and therefore contributes to the blocked condition (Pitts et al., 2017).

YO activation is initiated by reduced release of MIH from the XO/SG complex, which is mimicked by ESA. Increased ecdysteroid production by the activated YO in EP requires mTORC1-dependent protein synthesis. mTORC1 stimulates translation of mRNA by phosphorylation of eIF4E-binding protein (4E-BP) and p70 S6 kinase (S6K) (reviewed in Saxton and Sabatini, 2017). MIH inhibits protein synthesis in the YO, but has no effect on RNA synthesis (Soumoff and O'Connor, 1982; Mattson and Spaziani, 1986b). ESA increases protein synthesis and a transient increase in RNA synthesis in the YO (Simione and Hoffman, 1975; Gersch et al., 1977). Cycloheximide, an inhibitor of translation, but not actinomycin D, an inhibitor of transcription, inhibits protein synthesis and ecdysteroidogenesis in the YO (Mattson and Spaziani, 1986a; Mattson and Spaziani, 1986b); reviewed in Mattson, 1986).

A. MAP kinase signaling

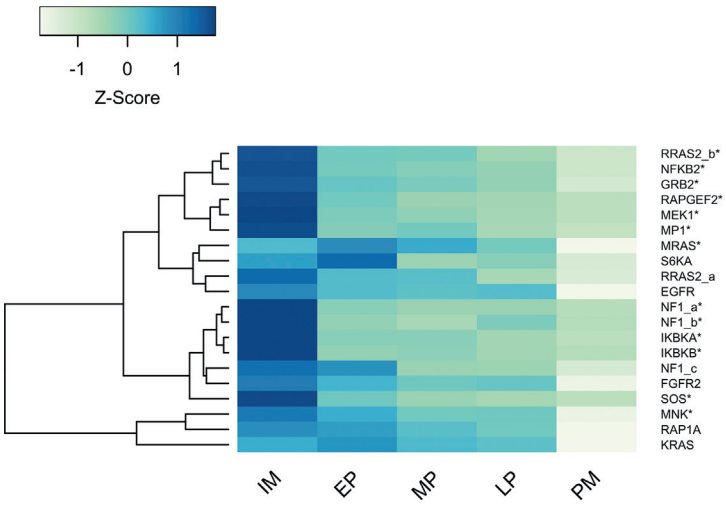

B. Notch signaling

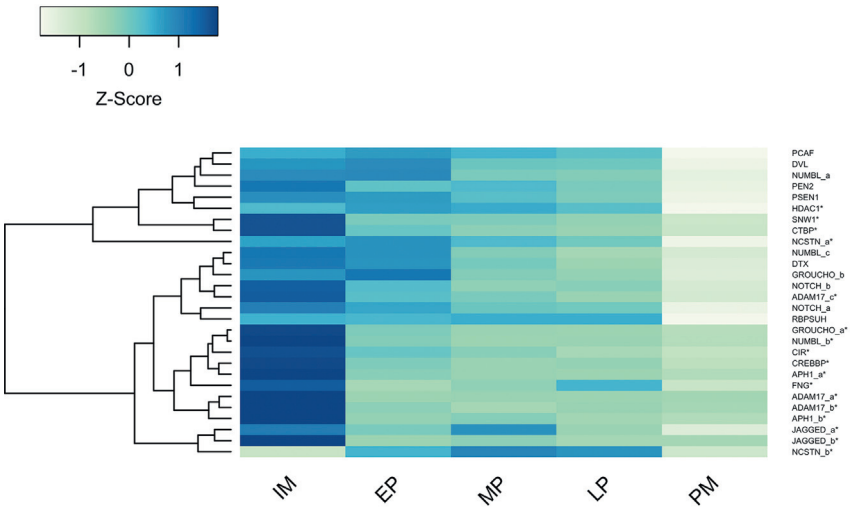

C. Wnt signaling

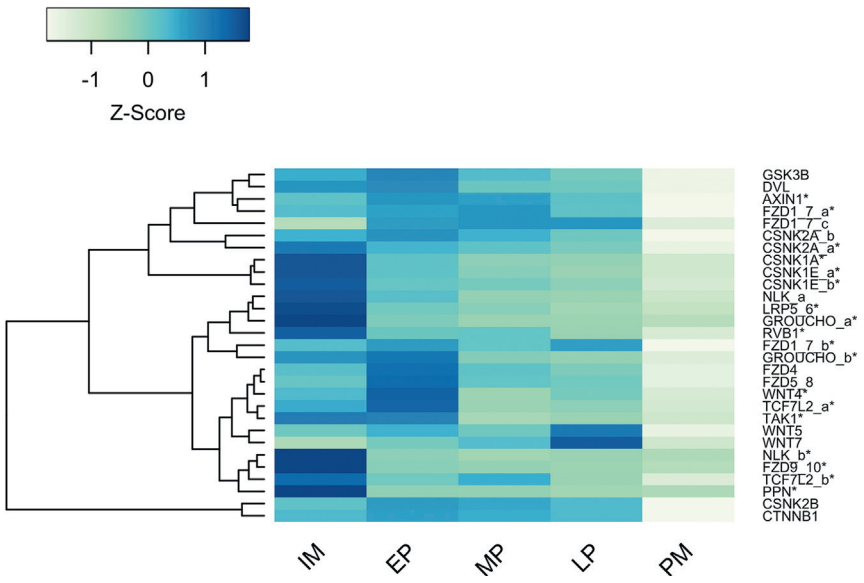

(caption on next page)

Fig. 7. Heatmap of the expression of genes in the MAP kinase (A), Notch (B), and Wnt (C) signaling pathways. DE contigs identified by limma-voom analyses are marked with an asterisk by the gene name. DE contigs identified by ANOVA are marked with a plus sign.

mTORC1 inhibitor rapamycin inhibits YO ecdysteroid synthesis and secretion (Abuhagr et al., 2014b; Abuhagr et al., 2016). Taken together, these data suggest that MIH signaling inhibits YO ecdysteroidogenesis by inhibiting mTORC1-dependent translation of mRNA into protein. Upon activation by reduced MIH, the increase in ecdysteroid synthetic capacity of the YO is due to an mTORC1-dependent increase in the global translation of mRNA to protein.

YO activation is also associated with the up-regulation of many genes in the mTOR signaling pathway. Molt induction of *G. lateralis* by MLA or ESA increases expression of mTOR signaling genes as measured by qPCR. In MLA animals, mRNA levels of *Gl-mTOR* and *Gl-Akt* are significantly increased in premolt, while molt stage has no effect on *Gl-Rheb* and *Gl-S6K* mRNA levels (Abuhagr et al., 2014b). In ESA animals, mRNA levels of *Gl-mTOR*, *Gl-Akt*, and *Gl-S6K* are increased by 3 days post-ESA, while ESA has no effect on *Gl-Rheb* mRNA level (Abuhagr et al., 2016). DEG analysis showed that many of the mTOR signaling genes were up-regulated in IM, EP, and MP stages (Fig. 5B; 6B). Expression of mTORC1 components *mTOR* and *Raptor* was sustained at high levels in IM, EP, and MP. *Rheb* GTPase, a key regulator of mTORC1 (reviewed in Heard et al., 2014), was expressed at high levels in EP and MP (Fig. 5B). As Rheb is not regulated post-translationally, *Rheb* mRNA level can be used as a proxy for Rheb protein activity. For example, knockdown of *Rheb* mRNA decreases mTORC1 activity in *Drosophila* S2 cells (Yang et al., 2006). Conversely, over-expression of *Rheb* stimulates mTORC1 activity and ecdysteroid synthesis in the *Drosophila* prothoracic gland (PG) (Layalle et al., 2008). Signaling components both upstream and downstream of mTORC1 were also differentially expressed (Fig. 8). TSC, which inactivates Rheb, is a dimer composed of TSC1/2. Two contigs encoding TSC2 (*tsc2_a* and *tsc2_b*) were identified in the YO transcriptome. The expression of *tsc2_a* was lower during premolt, while the expression of *tsc2_b* was higher during premolt (Fig. 5B, 6B). *Akt*, which inhibits TSC by phosphorylation, was expressed at higher levels in IM, EP, and MP (Fig. 5B, 6B). The mTORC1 substrates *S6K* and *EF4EBP* were expressed at high levels in IM and EP (Fig. 5B, 6B). Taken together, the DEG analysis indicates that the mTOR signaling pathway was up-regulated in IM and EP. This expression profile is consistent with the role of mTORC1-dependent protein synthesis and gene regulation in YO activation in EP and increased ecdysteroidogenesis in premolt.

The activin/TGFβ signaling pathway is involved in the transition of the YO from the activated state in EP (stage D_0) to the committed state in MP (stage D_1). Activation of activin/TGFβ signaling requires mTORC1 activity, as commitment is delayed 14 days in eyestalk-ablated *G. lateralis* injected with rapamycin (Abuhagr et al., 2016). The TGFβ superfamily is divided into four groups by ligands (BMP, TGFβ, Activin, and Nodal) and their respective membrane receptors (Fig. 8B; reviewed in Heldin and Moustakas, 2016; Luo, 2017). The activin/TGFβ signaling genes identified in the YO transcriptome are *Mstn*, *Activin receptor I* (*acvr1*), *Smad2/3* (*R-Smad*), *Smad4* (*Co-Smad*), *Smad6* (I-Smad), and *BAMBI* (Fig. 8B; Das et al., 2016); reviewed in Chaikuad and Bullock, 2016). *Mstn* is an activin-like member of the TGFβ family that was first characterized as a gene implicated in regulating protein turnover in *G. lateralis* muscle (Covi et al., 2008; Covi et al., 2010) and has subsequently been cloned from a variety of decapod species (reviewed in Chang and Mykles, 2011; Mykles and Medler, 2015). However, *Gl-Mstn* is also highly expressed in the YO and ESA increases *Gl-Mstn* mRNA levels 5.5-fold by 3 days post-ESA (Abuhagr et al., 2016). SB431542, an inhibitor of activin signaling, has no effect on YO activation in eyestalk-ablated *G. lateralis*, but prevents YO commitment and lowers *Gl-mTOR*, *Gl-Akt*, and *Gl-Rheb* mRNA levels in the YO (Abuhagr et al., 2016). DEG analysis showed higher expression of *Mstn* in IM, EP, and MP and higher expression of *Smad2/3* (*R-Smad*) and *Smad4* (*Co-Smad*) in EP and MP, while *acvr1* expression was unchanged (Fig. 5C, 6C). I-Smad (Smad6) and BAMBI are inhibitors of TGFβ signaling. I-Smad competitively associates with activated Type I receptors to block R-Smad activation, while BAMBI acts as a pseudoreceptor to TGFβ ligands (Fig. 8B; reviewed in Miyazawa and Miyazono, 2017). Expression of *Smad6* was unchanged in IM and premolt; by contrast, the expression of *BAMBI* dropped significantly from IM to EP (Fig. 5C, 6C). Collectively, these data indicate that the activin/TGFβ signaling pathway mediates YO commitment in MP.

DEG analysis identified additional three signaling pathways that regulate the molting glands of insects and crustaceans: MAP kinase, Notch, and Wnt (Table 2, Fig. 7). MAP kinase signaling has opposite effects on the molting glands of the two arthropod groups. In the *Drosophila* PG, PTTH binding to torso, a receptor tyrosine kinase, activates the MAP kinase pathway to stimulate ecdysteroid synthesis (reviewed in Covi et al., 2012; Niwa and Niwa, 2016; Rewitz et al., 2013; Yamanaka et al., 2013). In the *Scylla serrata* YO, MAP kinase signaling, as determined by ERK phosphorylation, is active in the PM and IM, when ecdysteroid synthesis is low (Imayavaramban et al., 2007). Inhibition of ERK phosphorylation with the MEK inhibitor PD98059 increases protein kinase C (PKC) activity, as well as the activities of two proteins involved in the transport and processing of cholesterol in the steroidogenic pathway (steroidogenic acute regulatory protein or StAR and cytochrome P450scc) in PM and IM (Imayavaramban et al., 2007). These data suggest that MAP kinase, with the involvement of PKC, inhibits YO ecdysteroidogenesis in PM and IM. However, the effects of activation of PKC with phorbol ester (PMA) are not consistent. PMA inhibits YO ecdysteroid synthesis in crayfish species (*Orconectes* sp.), but stimulates ecdysteroid synthesis in crab, *Cancer antennarius* (Mattson and Spaziani, 1987; Spaziani et al., 2001). The expression profile of MAP kinase signaling is not consistent with ERK phosphorylation observed in *S. serrata*: MAP kinase genes were up-regulated in IM but down-regulated in PM (Fig. 7A). The effects of MAP kinase and PKC signaling on ecdysteroid synthesis in the YO are distinct from the MIH signaling pathway (Spaziani et al., 2001), which suggests other factors beside MIH can regulate YO ecdysteroidogenesis. Those factors have not been identified.

Many of the components of the Notch and Wnt signaling pathways were differentially expressed over the molt cycle (Table 2, Fig. 7). Both Notch and Wnt mediate short-distance cell-cell communication via direct binding to a membrane ligand for Notch signaling or via autocrine or paracrine mechanisms for Wnt signaling (reviewed in Shimobayashi and Hall, 2014). Receptors for Wnt and Notch, as well as Hedgehog and Hippo, are highly expressed in the *Bombyx mori* PG (Alexandratos et al., 2016). In the *Drosophila* PG, genetic studies show that Wnt controls gene expression by way of Wnt-dependent *cis*-regulatory sequences (Archbold et al., 2014), Hippo/Warts signaling stimulates basal ecdysteroid synthesis (Moeller et al., 2017), and Hedgehog signaling inhibits ecdysteroid synthesis (Rodenfels et al., 2014). Notch, Wnt, and Hippo signaling pathways activate mTORC1 (reviewed in Shimobayashi and Hall, 2014). In mammals, there is extensive cross-talk between TGFβ/Smad and Notch and Wnt pathways with interactions that are determined by the cellular and developmental context (reviewed in Luo, 2017). Therefore, Notch and Wnt may coordinate ecdysteroid synthesis between YO cells by activating mTOR signaling directly and/or by activin/TGFβ signaling. To our knowledge, there are no studies on the functions of these pathways in the YO. In *Litopenaeus vannamei*, twelve Wnt genes are differentially expressed with developmental and molt stages, but expression in the YO was not examined (Du et al., 2018). The high expression of *Wnt5* and *Wnt7* in the LP YO (Fig. 7C) suggests that these ligands are involved with the peak in hemolymph ecdysteroid titers at the end of LP and repression of the YO in postmolt.

A. mTOR signaling pathway

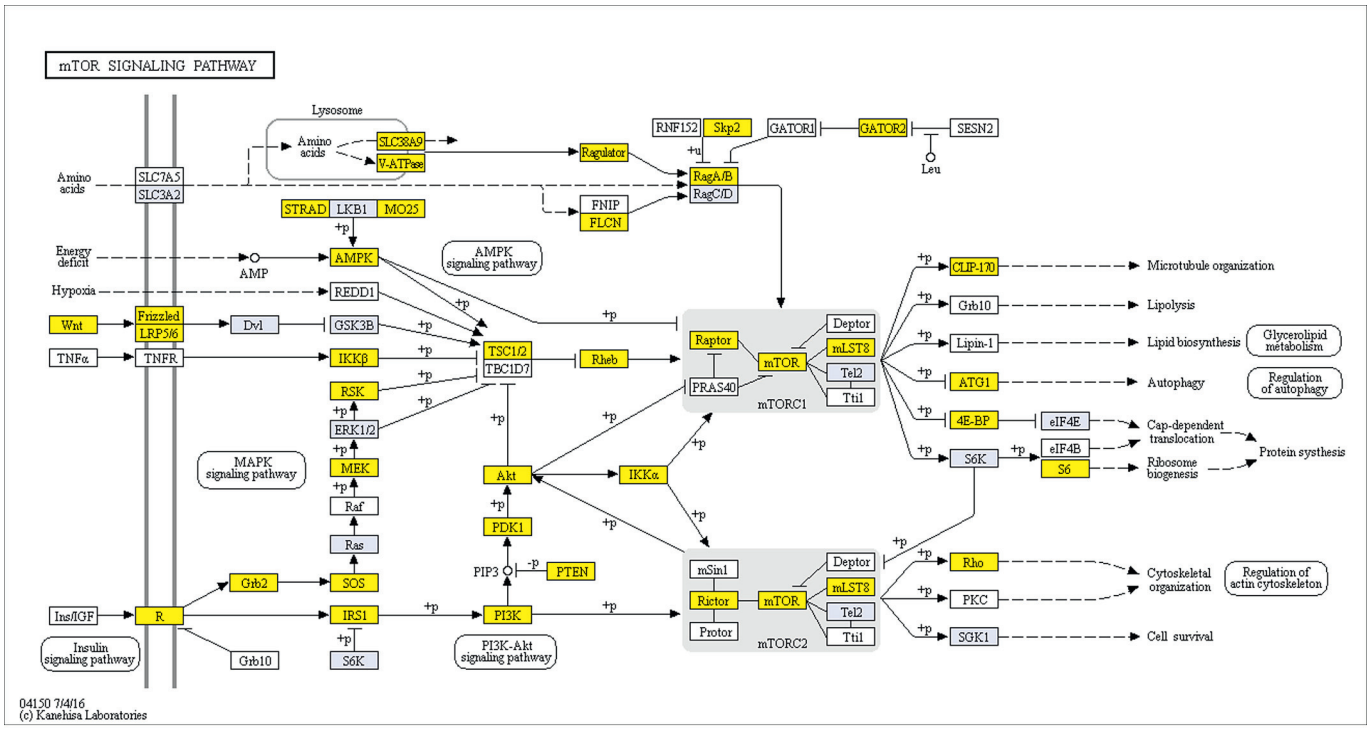

B. TGFβ signaling pathway

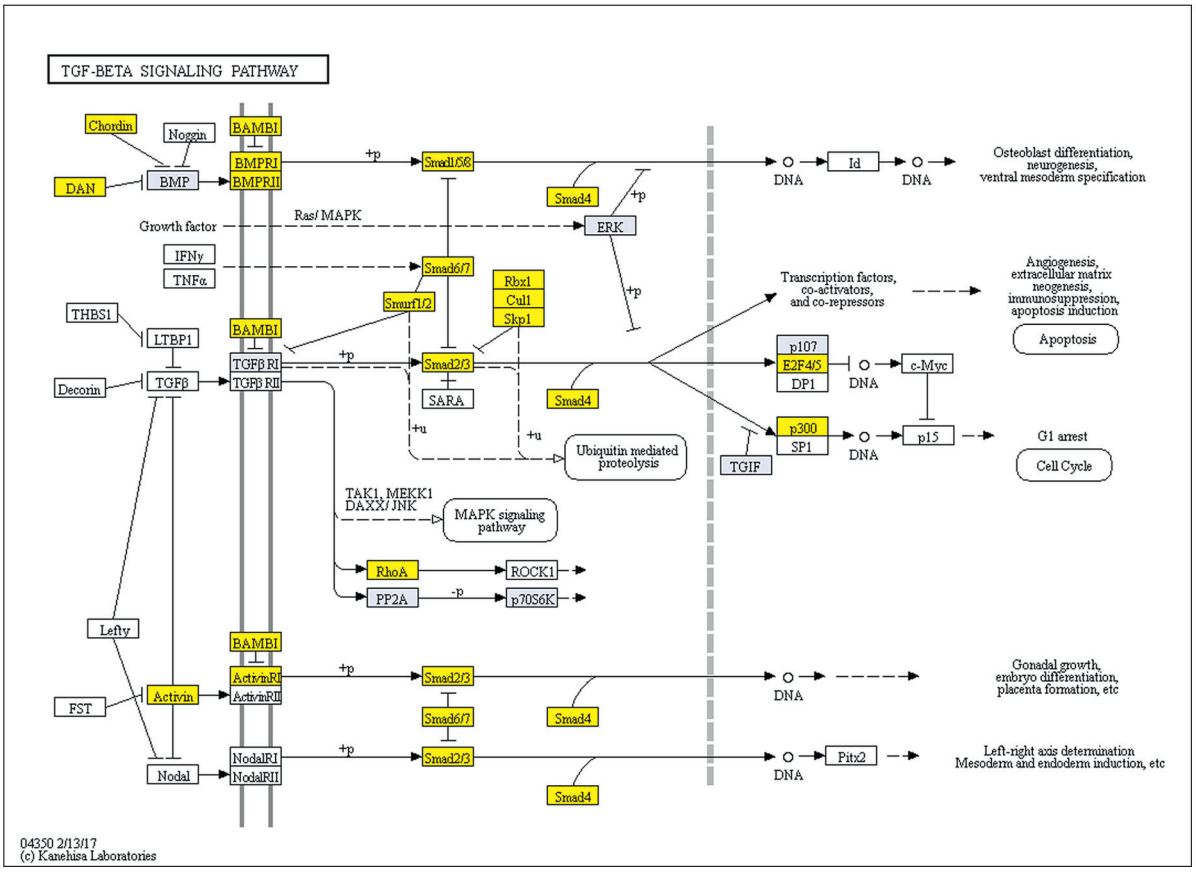

(caption on next page)

Fig. 8. KEGG pathways for mTOR (A) and TGFβ (B). Boxes with lavender shading are pathway components identified in YO transcriptome that were not differentially expressed. Boxes with yellow shading identify components that were differentially expressed via ANOVA and limma-voom analyses. (For interpretation of the references to colour in this figure legend, the reader is referred to the web version of this article.)

Investigation of Notch, Wnt, Hedgehog, and Hippo pathways will certainly provide new insights into how the YO integrates various intrinsic and extrinsic signals.

RNA-Seq data was used as a tool for the identification of 24 genes associated with specific molt stages. Using expression profiles and the percentage of DE contigs in the KEGG analysis as criteria, 11 signaling genes were up-regulated in EP, and therefore associated with YO activation (Tables 3, S3). These genes are components of the AMPK, PI3K-Akt, MAPK, calcium, Hippo, Wnt, and Notch signaling pathways. A common target of these signaling pathways is mTOR (reviewed in Huang and Fingar, 2014; Laplante and Sabatini, 2012; Shimobayashi and Hall, 2014). Other genes were identified as characteristic of the other molt stages: five genes in MP, four genes in LP, and four genes in PM (Table 3, S4). Collectively, the expression of these genes could be used a diagnostic markers for determining the effects of molt manipulation (e.g., ESA, MLA, and limb bud autotomy) and experimental treatments (e.g., rapamycin and SB431542) on the physiological state of the YO.

5. Conclusions

The MIH, mTOR, and activin/TGFβ signaling pathways regulate the physiological properties of the YO. Fig. 9 summarizes the results from this study and from previous studies (Abuhagr et al., 2014b; Abuhagr et al., 2016; Das et al., 2016; Das and Mykles, 2016; Shyamal et al., 2018). The pulsatile release of MIH from the XO/SG complex initiates a cyclic nucleotide cascade that inhibits mTORC1 activity, possibly mediated by cGMP-dependent protein kinase (*pkg*), and maintains the YO in the basal state (reviewed in Chang and Mykles, 2011; Covi et al., 2012; Mykles et al., 2010). Reduction of MIH release de-represses the YO; mTORC1-dependent protein synthesis drives YO hypertrophy and increased ecdysteroidogenic capacity and the animal enters EP (Das et al., 2016); reviewed in Chang and Mykles, 2011). In insects, mTOR, either via prothoracicotropic hormone (PTTH) or insulin signaling, is required for ecdysteroid synthesis in the PG (Danielsen et al., 2016; Das et al., 2016); reviewed in Covi et al., 2012; Niwa and Niwa, 2016; Rewitz et al., 2013; Yamanaka et al., 2013). The activated YO increases the expression of *Mstn* (Fig. 5C; Abuhagr et al., 2016), activating the activin/TGFβ signaling pathway to drive the transition of the YO to the committed state. The critical role of *Mstn* in the EP/MP transition may explain the effects of injecting *Mstn* dsRNA constructs on molting in three shrimp species. Down-regulation of *Mstn* with RNAi lengthens the intermolt interval in *Fenneropenaeus merguiensis* (Zhuo et al., 2017), *Penaeus monodon* (De Santis et al., 2011), and L. *vannamei* (Lee et al., 2015). Although YO *Mstn* expression was not examined in these studies, knocking down the expression of *Mstn* in the YO could have delayed progression from EP to MP, resulting in a lengthened intermolt interval. In insects, activin/TGFβ signaling mediates PG transitions and responsiveness to PTTH during development (Gibbens et al., 2011; Das et al., 2016); reviewed in Niwa and Niwa, 2016; Rewitz et al., 2013; Yamanaka et al., 2013). The data suggest that there is a negative feedback between mTOR and MIH signaling and a positive feedback between activin/TGFβ and mTOR signaling (Fig. 9). The activation of mTORC1 coincides with the down-regulation of MIH signaling genes in EP (Figs. 5A, 6A) and up-regulation of the activin/TGFβ signaling genes in EP and MP (Fig. 5C, 6C). Moreover, blocking activin/TGFβ signaling with SB431542 decreases expression of *Gl-mTOR*, *Gl-Akt*, and *Gl-Rheb* in the YO (Abuhagr et al., 2016).

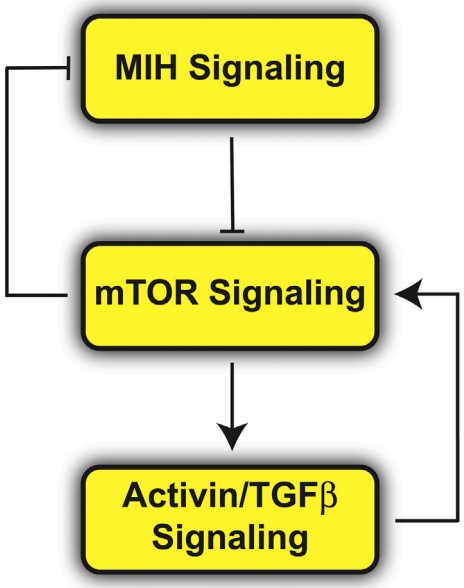

Fig. 9. Molt-cycle-dependent regulation of the MIH, mTOR, and Activin/TGFβ signaling pathways in the Y-organ. During intermolt, MIH signaling inhibits mTOR signaling to maintain the YO in the basal state. Reduction in MIH de-represses the YO by activating mTOR and the YO transitions to the activated state in early premolt. mTOR signaling up-regulates Activin/TGFβ signaling and the YO transitions to the committed state in mid premolt. Negative feedback by mTOR down-regulates MIH signaling, reducing the sensitivity of the YO to MIH in mid and late premolt. Positive feedback by Activin/TGFβ signaling up-regulates mTOR to support increased ecdysteroid synthesis in mid and late premolt.

The mechanisms underlying the repression of the YO in the LP/PM transition and the restoration of the YO to the basal state in the PM/IM transition require further study. It is hypothesized that the peak in hemolymph ecdysteroid titer at the end of premolt triggers the repressed state (reviewed in Chang and Mykles, 2011), although the higher expression of *Wnt5* and *Wnt7* in LP (Fig. 7C) suggests that Wnt signaling may play a role. Among the significant findings reported here are that the YO remains in the repressed state at least through 10 days post-ecdysis (stage B) and that relative gene expression is low in the repressed YO (Table S2; Figs. 4, 5). During postmolt (stages A, B, and C_{1-3}), synthesis and calcification of the exoskeleton continues as the endocuticle is deposited; synthesis of the exoskeleton is completed with the deposition of the membranous layer (reviewed in Skinner, 1985). Hemolymph ecdysteroid titers are at their lowest in PM (reviewed in Mykles, 2011), which indicates low ecdysteroid synthesis by the YO. A repressed YO may assure that precocious molting does not occur while the exoskeleton is still being synthesized. This means that the transition of the YO back to the basal state, which is inhibited by MIH and is capable of activation by reduced MIH, occurs between stage B and stage C_4 (IM). A transcriptomics approach may reveal signaling pathways that restore the YO to the basal state, which is characterized by higher expression of MIH, BMP/TGFβ, MAP kinase, Notch, and Wnt signaling genes. This and recent studies using transcriptomics of the crustacean and insect molting glands have revealed complex interactions between signaling pathways that integrate the actions of nutrients, growth factors, and hormones on ecdysteroidogenesis with tissue regeneration, developmental stage, and environmental cues to coordinate organismal growth and organ size (Alexandratos et al., 2016; Danielsen et al., 2016; Das et al., 2016; Christesen et al., 2017; Nakaoka et al., 2017; Shyamal et al., 2018).

The reference YO transcriptome (Fig. 1) is available for download

from CyVerse, which is supported by the National Science Foundation under Award Numbers DBI-0735191 and DBI-1265383 (http://www.cyverse.org). The public sharing link is: https://de.cyverse.org/dl/d/E9DC31DA-CB6E-4C2E-A511-510D867B0A20/Glat_MLA_reference_transcriptome.fasta.gz.

The expression data (count and FPKM), and KEGG annotation of contigs from the filtered YO dataset (Fig. 1) can be downloaded from: https://de.cyverse.org/dl/d/5F864EB3-7E48-4775-B983-DE39E488FFDC/FilteredTranscriptomeData.xlsx.zip. Supplementary data to this article can be found online at doi:https://doi.org/10.1016/j.cbd.2018.06.001.

Acknowledgments

We thank Dr. Ernest S. Chang and Sharon A. Chang, UC Davis Bodega Marine Laboratory, for ELISA on hemolymph samples; Hector C. Horta for collecting *G. lateralis*; Dr. Tomer Ventura, University of the Sunshine Coast, for critical reading of the manuscript; and Graham Wiley, Oklahoma Medical Research Facility, for Illumina sequencing. We acknowledge the assistance of Jesse Schafer, Oklahoma State University High Performance Computing Center (National Science Foundation grant OCI–1126330), for technical support. We also thank Clayton Hallman for his assistance with statistical analysis of the transcriptome data using R. We thank the staff of Consejo Dominicano de Pesca y Acuicultura, Dominican Republic, for expediting approval of permits and identifying suitable sites for collecting *G. lateralis*. This project was supported by the National Science Foundation (IOS-1257732).

References

Abuhagr, A.M., Blindert, J.L., Nimitkul, S., Zander, I.A., LaBere, S.M., Chang, S.A., MacLea, K.S., Chang, E.S., Mykles, D.L., 2014a. Molt regulation in green and red color morphs of the crab *Carcinus maenas*: gene expression of molt-inhibiting hormone signaling components. J. Exp. Biol. 217, 796–808.

Abuhagr, A.M., MacLea, K.S., Chang, E.S., Mykles, D.L., 2014b. Mechanistic target of rapamycin (mTOR) signaling genes in decapod crustaceans: cloning and tissue expression of mTOR, Akt, Rheb, and p70 S6 kinase in the green crab, *Carcinus maenas*, and blackback land crab, *Gecarcinus lateralis*. Comp. Biochem. Physiol. 168A, 25–39.

Abuhagr, A.M., MacLea, K.S., Mudron, M.R., Chang, S.A., Chang, E.S., Mykles, D.L., 2016. Roles of mechanistic target of rapamycin and transforming growth factor-beta signaling in the molting gland (Y-organ) of the blackback land crab, *Gecarcinus lateralis*. Comp. Biochem. Physiol. 198A, 15–21.

Aiken, D.E., Waddy, S.L., 1992. The growth process in crayfish. Rev. Aquat. Sci. 6, 335–381.

Alexandratos, A., Moulos, P., Nellas, I., Mavridis, K., Dedos, S.G., 2016. Reassessing ecdysteroidogenic cells from the cell membrane receptors' perspective. Sci. Rep. 6, 20229.

Andersen, D.S., Colombani, J., Leopold, P., 2013. Coordination of organ growth: principles and outstanding questions from the world of insects. Trends Cell Biol. 23, 336–344.

Andrews, A.G., 2010. FastQC: A Quality Control Tool for High Throughput Sequence Data (Available online at:). http://www.bioinformatics.babraham.ac.uk/projects/fastqc/.

Archbold, H.C., Broussard, C., Chang, M.V., Cadigan, K.M., 2014. Bipartite recognition of DNA by TCF/pangolin is remarkably flexible and contributes to transcriptional responsiveness and tissue specificity of wingless signaling. PLoS Genet. 10, e1004591.

Bolger, A.M., Lohse, M., Usadel, B., 2014. Trimmomatic: a flexible trimmer for Illumina sequence data. Bioinformatics 30, 2114–2120.

Chaikuad, A., Bullock, A.N., 2016. Structural basis of intracellular TGF-beta signaling: receptors and Smads. Cold Spring Harb. Perspect. Biol. 8, a022111.

Chang, E.S., Mykles, D.L., 2011. Regulation of crustacean molting: a review and our perspectives. Gen. Comp. Endocrinol. 172, 323–330.

Christesen, D., Yang, Y.T., Somers, J., Robin, C., Sztal, T., Batterham, P., Perry, T., 2017. Transcriptome analysis of *Drosophila melanogaster* third instar larval ring glands points to novel functions and uncovers a cytochrome P450 required for development. G3-Genes Genomes Genetics 7, 467–479.

Chung, J.S., Webster, S.G., 2003. Moult cycle-related changes in biological activity of moult-inhibiting hormone (MIH) and crustacean hyperglycaemic hormone (CHH) in the crab, *Carcinus maenas*. From target to transcript. Eur. J. Biochem. 270, 3280–3288.

Covi, J.A., Kim, H.W., Mykles, D.L., 2008. Expression of alternatively spliced transcripts for a myostatin-like protein in the blackback land crab, *Gecarcinus lateralis*. Comp. Biochem. Physiol. 150A, 423–430.

Covi, J.A., Chang, E.S., Mykles, D.L., 2009. Conserved role of cyclic nucleotides in the regulation of ecdysteroidogenesis by the crustacean molting gland. Comp. Biochem. Physiol. 152A, 470–477.

Covi, J.A., Bader, B.D., Chang, E.S., Mykles, D.L., 2010. Molt cycle regulation of protein synthesis in skeletal muscle of the blackback land crab, *Gecarcinus lateralis*, and the differential expression of a myostatin-like factor during atrophy induced by molting or unweighting. J. Exp. Biol. 213, 172–183.

Covi, J.A., Chang, E.S., Mykles, D.L., 2012. Neuropeptide signaling mechanisms in crustacean and insect molting glands. Invertebr. Reprod. Dev. 56, 33–49.

Danielsen, E.T., Moeller, M.E., Yamanaka, N., Ou, Q.X., Laursen, J.M., Soenderholm, C., Zhuo, R., Phelps, B., Tang, K., Zeng, J., Kondo, S., Nielsen, C.H., Harvald, E.B., Faergeman, N.J., Haley, M.J., O'Connor, K.A., King-Jones, K., O'Connor, M.B., Rewitz, K.F., 2016. A *Drosophila* genome-wide screen identifies regulators of steroid hormone production and developmental timing. Dev. Cell 37, 558–570.

Das, S., Mykles, D.L., 2016. A comparison of resources for the annotation of a *de novo* assembled transcriptome in the molting gland (Y-organ) of the blackback land crab, *Gecarcinus lateralis*. Integr. Comp. Biol. 56, 1103–1112.

Das, S., Pitts, N.L., Mudron, M.R., Durica, D.S., Mykles, D.L., 2016. Transcriptome analysis of the molting gland (Y-organ) from the blackback land crab, *Gecarcinus lateralis*. Comp. Biochem. Physiol. 17D, 26–40.

De Santis, C., Wade, N.M., Jerry, D.R., Preston, N.P., Glencross, B.D., Sellars, M.J., 2011. Growing backwards: an inverted role for the shrimp ortholog of vertebrate myostatin and GDF11. J. Exp. Biol. 214, 2671–2677.

DeLalio, L.J., Dion, S.M., Bootes, A.M., Smith, W.A., 2015. Direct effects of hypoxia and nitric oxide on ecdysone secretion by insect prothoracic glands. J. Insect Physiol. 76, 56–66.

Du, J.L., Zhang, X.J., Yuan, J.B., Zhang, X.O., Li, F.H., Xiang, J.H., 2018. Wnt gene family members and their expression profiling in *Litopenaeus vannamei*. Fish Shellfish Immunol. 77, 233–243.

Fu, L.M., Niu, B.F., Zhu, Z.W., Wu, S.T., Li, W.Z., 2012. CD-HIT: accelerated for clustering the next-generation sequencing data. Bioinformatics 28, 3150–3152.

Gersch, M., Richter, K., Eibisch, H., 1977. Studies on characterization and action of molt-inhibiting hormone (MIH) of sinus gland in *Orconectes limosus* Rafinesque (Crustacea-Decapoda). Zool. Jb. Physiol. Bd. 81, 133–152.

Gibbens, Y.Y., Warren, J.T., Gilbert, L.I., O'Connor, M.B., 2011. Neuroendocrine regulation of *Drosophila* metamorphosis requires TGF beta/activin signaling. Development 138, 2693–2703.

Grabherr, M.G., Haas, B.J., Yassour, M., Levin, J.Z., Thompson, D.A., Amit, I., Adiconis, X., Fan, L., Raychowdhury, R., Zeng, Q.D., Chen, Z.H., Mauceli, E., Hacohen, N., Gnirke, A., Rhind, N., di Palma, F., Birren, B.W., Nusbaum, C., Lindblad-Toh, K., Friedman, N., Regev, A., 2011. Full-length transcriptome assembly from RNA-Seq data without a reference genome. Nat. Biotechnol. 29, 644–652.

Green, B.S., Gardner, C., Hochmuth, J.D., Linnane, A., 2014. Environmental effects on fished lobsters and crabs. Rev. Fish Biol. Fish. 24, 613–638.

Hackney, J.F., Cherbas, P., 2014. Injury response checkpoint and developmental timing in insects. Flying 8, 226–231.

Heard, J.J., Fong, V., Bathaie, S.Z., Tamanoi, F., 2014. Recent progress in the study of the Rheb family GTPases. Cell. Signal. 26, 1950–1957.

Heldin, C.H., Moustakas, A., 2016. Signaling receptors for TGF-beta family members. Cold Spring Harb. Perspect. Biol. 8, a022053.

Hopkins, P.M., 2012. The eyes have it: a brief history of crustacean neuroendocrinology. Gen. Comp. Endocrinol. 175, 357–366.

Hopkins, P.M., Das, S., 2015. Regeneration in crustaceans. In: Chang, E.S., Thiel, M. (Eds.), Physiology. Vol. 4. Oxford University Press, Oxford, U.K., pp. 168–198.

Huang, K.Z., Fingar, D.C., 2014. Growing knowledge of the mTOR signaling network. Semin. Cell Dev. Biol. 36, 79–90.

Huson, D.H., Auch, A.F., Qi, J., Schuster, S.C., 2007. MEGAN analysis of metagenomic data. Genome Res. 17, 377–386.

Imayavaramban, L., Dhayaparan, D., Devaraj, H., 2007. Molecular mechanism of molt-inhibiting hormone (MIH) induced suppression of ecdysteroidogenesis in the Y-organ of mud crab: *Scylla serrata*. FEBS Lett. 581, 5167–5172.

Jaszczak, J.S., Wolpe, J.B., Dao, A.Q., Halme, A., 2015. Nitric oxide synthase regulates growth coordination during *Drosophila melanogaster* imaginal disc regeneration. Genetics 200, 1219–1228.

Jaszczak, J.S., Wolpe, J.B., Bhandari, R., Jaszczak, R.G., Halme, A., 2016. Growth coordination during *Drosophila melanogaster* imaginal disc regeneration is mediated by signaling through the relaxin receptor Lgr3 in the prothoracic gland. Genetics 204, 703–709.

Kim, H.W., Batista, L.A., Hoppes, J.L., Lee, K.J., Mykles, D.L., 2004. A crustacean nitric oxide synthase expressed in nerve ganglia, Y-organ, gill and gonad of the tropical land crab, *Gecarcinus lateralis*. J. Exp. Biol. 207, 2845–2857.

Langmead, B., Salzberg, S.L., 2012. Fast gapped-read alignment with bowtie 2. Nat. Methods 9, 357–359.

Laplante, M., Sabatini, D.M., 2012. mTOR signaling in growth control and disease. Cell 149, 274–293.

Law, C.W., Chen, Y.S., Shi, W., Smyth, G.K., 2014. Voom: precision weights unlock linear model analysis tools for RNA-seq read counts. Genome Biol. 15, R29.

Layalle, S., Arquier, N., Leopold, P., 2008. The TOR pathway couples nutrition and developmental timing in *Drosophila*. Dev. Cell 15, 568–577.

Lee, S.G., Mykles, D.L., 2006. Proteomics and signal transduction in the crustacean molting gland. Integr. Comp. Biol. 46, 965–977.

Lee, S.G., Bader, B.D., Chang, E.S., Mykles, D.L., 2007a. Effects of elevated ecdysteroid on tissue expression of three guanylyl cyclases in the tropical land crab *Gecarcinus lateralis*: possible roles of neuropeptide signaling in the molting gland. J. Exp. Biol. 210, 3245–3254.

Lee, S.G., Kim, H.W., Mykles, D.L., 2007b. Guanylyl cyclases in the tropical land crab, *Gecarcinus lateralis*: cloning of soluble (NO-sensitive and -insensitive) and membrane receptor forms. Comp. Biochem. Physiol. 2D, 332–344.

Lee, J.H., Momani, J., Kim, Y.M., Kang, C.K., Choi, J.H., Baek, H.J., Kim, H.W., 2015.

Effective RNA-silencing strategy of Lv-MSTN/GDF11 gene and its effects on the growth in shrimp, *Litopenaeus vannamei*. Comp. Biochem. Physiol. 179B, 9–16.
Leek, J.T., Storey, J.D., 2007. Capturing heterogeneity in gene expression studies by surrogate variable analysis. PLoS Genet. 3, 1724–1735.
Luo, K., 2017. Signaling cross talk between TGF-beta/Smad and other signaling pathways. Cold Spring Harb. Perspect. Biol. 9, a022137.
MacLea, K.S., Abuhagr, A.M., Pitts, N.L., Covi, J.A., Bader, B.D., Chang, E.S., Mykles, D.L., 2012. Rheb, an activator of target of rapamycin, in the blackback land crab, *Gecarcinus lateralis*: cloning and effects of molting and unweighting on expression in skeletal muscle. J. Exp. Biol. 215, 590–604.
Mattson, M.P., 1986. New insights into neuroendocrine regulation of the crustacean molt cycle. Zool. Sci. 3, 733–744.
Mattson, M.P., Spaziani, E., 1986a. Regulation of crab Y-organ steroidogenesis *in vitro* - evidence that ecdysteroid production increases through activation of cAMP-phosphodiesterase by calcium-calmodulin. Mol. Cell. Endocrinol. 48, 135–151.
Mattson, M.P., Spaziani, E., 1986b. Regulation of Y-organ ecdysteroidogenesis by molt-inhibiting hormone in crabs: involvement of cyclic AMP-mediated protein synthesis. Gen. Comp. Endocrinol. 63, 414–423.
Mattson, M.P., Spaziani, E., 1987. Demonstration of protein kinase C activity in crustacean Y-organs. And partial definition of its role in regulation of ecdysteroidogenesis. Mol. Cell. Endocrinol. 49, 159–171.
Miyazawa, K., Miyazono, K., 2017. Regulation of TGF-beta family signaling by inhibitory smads. Cold Spring Harb. Perspect. Biol. 9, a022095.
Moeller, M.E., Nagy, S., Gerlach, S.U., Soegaard, K.C., Danielsen, E.T., Texada, M.J., Rewitz, K.F., 2017. Warts signaling controls organ and body growth through regulation of ecdysone. Curr. Biol. 27, 1652–1659.
Mykles, D.L., 2001. Interactions between limb regeneration and molting in decapod crustaceans. Am. Zool. 41, 399–406.
Mykles, D.L., 2011. Ecdysteroid metabolism in crustaceans. J. Steroid Biochem. Mol. Biol. 127, 196–203.
Mykles, D.L., Medler, S., 2015. Skeletal muscle differentiation, growth, and plasticity. In: Chang, E.S., Thiel, M. (Eds.), The Natural History of the Crustacea: Physiology. Vol. 4. Oxford University Press, Oxford, U.K., pp. 134–167.
Mykles, D.L., Adams, M.E., Gade, G., Lange, A.B., Marco, H.G., Orchard, I., 2010. Neuropeptide action in insects and crustaceans. Physiol. Biochem. Zool. 83, 836–846.
Mykles, D.L., Burnett, K.G., Durica, D.S., Stillman, J.H., 2016. Tapping the power of crustacean transcriptomics to address grand challenges in comparative biology: an introduction to the symposium. Integr. Comp. Biol. 56, 1047–1054.
Nakaoka, T., Iga, M., Yamada, T., Koujima, I., Takeshima, M., Zhou, X.Y., Suzuki, Y., Ogihara, M.H., Kataoka, H., 2017. Deep sequencing of the prothoracic gland transcriptome reveals new players in insect ecdysterodogenesis. PLoS One 12, e0172951.
Nakatsuji, T., Sonobe, H., 2004. Regulation of ecdysteroid secretion from the Y-organ by molt-inhibiting hormone in the American crayfish, *Procambarus clarkii*. Gen. Comp. Endocrinol. 135, 358–364.
Nakatsuji, T., Sonobe, H., Watson, R.D., 2006. Molt-inhibiting hormone-mediated regulation of ecdysteroid synthesis in Y-organs of the crayfish (*Procambarus clarkii*): involvement of cyclic GMP and cycle nucleotide phosphodiesterase. Mol. Cell. Endocrinol. 253, 76–82.
Nakatsuji, T., Lee, C.Y., Watson, R.D., 2009. Crustacean molt-inhibiting hormone: structure, function, and cellular mode of action. Comp. Biochem. Physiol. 152A, 139–148.
Niwa, Y.S., Niwa, R., 2016. Transcriptional regulation of insect steroid hormone biosynthesis and its role in controlling timing of molting and metamorphosis. Develop. Growth Differ. 58, 94–105.
Pitts, N.L., Schulz, H.M., Oatman, S.R., Mykles, D.L., 2017. Elevated expression of neuropeptide signaling genes in the eyestalk ganglia and Y-organ of *Gecarcinus lateralis* individuals that are refractory to molt induction. Comp. Biochem. Physiol. 214B, 66–78.
Rewitz, K.F., Yamanaka, N., O'Connor, M.B., 2013. Developmental checkpoints and feedback circuits time insect maturation. In: Shi, Y.B. (Ed.), Animal Metamorphosis. 103. pp. 1–33.
Risso, D., Ngai, J., Speed, T.P., Dudoit, S., 2014. Normalization of RNA-seq data using factor analysis of control genes or samples. Nat. Biotechnol. 32, 896–902.
Ritchie, M.E., Phipson, B., Wu, D., Hu, Y.F., Law, C.W., Shi, W., Smyth, G.K., 2015. Limma powers differential expression analyses for RNA-sequencing and microarray studies. Nucleic Acids Res. 43, e47.
Roberts, A., Pachter, L., 2013. Streaming fragment assignment for real-time analysis of sequencing experiments. Nat. Methods 10, 71–73.
Robinson, M.D., McCarthy, D.J., Smyth, G.K., 2010. edgeR: a bioconductor package for differential expression analysis of digital gene expression data. Bioinformatics 26, 139–140.
Rodenfels, J., Lavrynenko, O., Aycirex, S., Sampaio, J.L., Carvalho, M., Shevchenko, A., Eaton, S., 2014. Production of systemically circulating hedgehog by the intestine couples nutrition to growth and development. Genes Dev. 28, 2636–2651.
Saxton, R.A., Sabatini, D.M., 2017. mTOR signaling in growth, metabolism, and disease. Cell 168, 960–976.
Shimobayashi, M., Hall, M.N., 2014. Making new contacts: the mTOR network in metabolism and signalling crosstalk. Nat. Rev. Mol. Cell Biol. 15, 155–162.
Shyamal, S., Das, S., Guruacharya, A., Mykles, D.L., Durica, D.S., 2018. Transcriptomic analysis of crustacean molting gland (Y-organ) regulation via the mTOR signaling pathway. Sci. Rep. 8, 7307.
Simione, F.P., Hoffman, D.L., 1975. Some effects of eyestalk removal on the Y-organs of *Cancer irroratus* Say. Biol. Bull. 148, 440–447.
Skinner, D.M., 1985. Molting and regeneration. In: Bliss, D.E., Mantel, L.H. (Eds.), The Biology of Crustacea. Academic Press, New York, pp. 43–146.
Soumoff, C., O'Connor, J.D., 1982. Repression of Y-organ secretory activity by molt-inhibiting hormone in the crab *Pachygrapsus crassipes*. Gen. Comp. Endocrinol. 48, 432–439.
Spaziani, E., Jegla, T.C., Wang, W.L., Booth, J.A., Connolly, S.M., Conrad, C.C., Dewall, M.J., Sarno, C.M., Stone, D.K., Montgomery, R., 2001. Further studies on signaling pathways for ecdysteroidogenesis in crustacean Y-organs. Am. Zool. 41, 418–429.
Tom, M., Manfrin, C., Giulianini, P.G., Pallavicini, A., 2013. Crustacean oxi-reductases protein sequences derived from a functional genomic project potentially involved in ecdysteroid hormones metabolism - a starting point for function examination. Gen. Comp. Endocrinol. 194, 71–80.
Webster, S.G., 2015. Endocrinology of molting. In: Chang, E.S., Thiel, M. (Eds.), Physiology. Vol. 4. Oxford Press, Oxford, pp. 1–35.
Webster, S.G., Keller, R., Dircksen, H., 2012. The CHH-superfamily of multifunctional peptide hormones controlling crustacean metabolism, osmoregulation, moulting, and reproduction. Gen. Comp. Endocrinol. 175, 217–233.
Xie, C., Mao, X.Z., Huang, J.J., Ding, Y., Wu, J.M., Dong, S., Kong, L., Gao, G., Li, C.Y., Wei, L.P., 2011. KOBAS 2.0: a web server for annotation and identification of enriched pathways and diseases. Nucleic Acids Res. 39, W316–W322.
Yamanaka, N., Rewitz, K.F., O'Connor, M.B., 2013. Ecdysone control of developmental transitions: Lessons from *Drosophila* research. In: Berenbaum, M.R. (Ed.), Ann. Rev. Entomol. Vol. 58. pp. 497–516.
Yang, Q., Inoki, K., Kim, E., Guan, K.L., 2006. TSC1/TSC2 and Rheb have different effects on TORC1 and TORC2 activity. Proc. Natl. Acad. Sci. U. S. A. 103, 6811–6816.
Yu, X.L., Chang, E.S., Mykles, D.L., 2002. Characterization of limb autotomy factor-proecdysis (LAF_{pro}), isolated from limb regenerates, that suspends molting in the land crab *Gecarcinus lateralis*. Biol. Bull. 202, 204–212.
Zhuo, R.Q., Zhou, T.T., Yang, S.P., Chan, S.M.F., 2017. Characterization of a molt-related myostatin gene (FmMstn) from the banana shrimp *Fenneropenaeus merguiensis*. Gen. Comp. Endocrinol. 248, 55–68.